AGE, PROVENANCE, AND GEOCHEMICAL RELATIONSHIPS AMONGST THE GREAT VALLEY GROUP, COAST RANGE OPHIOLITE, AND FRANCISCAN SUBDUCTION COMPLEX AT DEL PUERTO CANYON, CENTRAL CALIFORNIA

by

Natalee Emma Weis

A thesis submitted in partial fulfillment
of the requirements for the degree

of

Master of Science

in

Earth Sciences

MONTANA STATE UNIVERSITY
Bozeman, Montana

May 2024

DEDICATION

This thesis is dedicated to Frank Mikan for inspiring all who are fortunate enough to enter his classroom, for introducing me to geology, and for giving me the rock hammer that I used to collect the samples in this study. This work is in honor of Grandma (Joan Anderson) and Joji Weis who are with me always, especially while outside looking at rocks. Thank you to Mom, Dad, Reyden Weis, Meemaw, Dadu, and Ian Nielsen for your endless support and encouragement.

ACKNOWLEDGEMENTS

Devon A. Orme, Kathleen D. Surpless, and Andrew K. Laskowski provided initial edits to this thesis, and Jim Crowley, Nicole Stine, Ian Colliver, Carly Ross, and Emma Sweet supported this research during field and lab work. Funding was provided by the National Science Foundation (NSF) grant EAR-CAREER-1942460 to Devon A. Orme. We are grateful to the landowners in Del Puerto Canyon for graciously allowing us to visit their properties and to collect samples from their land. Thank you to the California Well Sample Repository, specifically Charles and Leon, for sample collection assistance, the University of Arizona Laserchron Center and Staff for analytical support (NSF EAR-1649254), ZirChron for assistance with mineral separation, Washington State University for geochemical analyses, and Spectrum Petrographics for thin sections. We are thankful for Dr. Kurt Sundell for his assistance with Lu-Hf data reduction and help with MatLab programs, Zachary Morrow, Natali Kragh, and Rebekah Kennedy for discussions regarding petrography and geochemistry.

TABLE OF CONTENTS

TABLE OF CONTENTS CONTINUED

LIST OF TABLES

Table Page

LIST OF FIGURES

Figure Page

ABSTRACT

The Great Valley Forearc (GVF) basin of California preserves an extensive rock record of subduction zone processes, including evidence for the earliest states of forearc evolution. During initiation of the basin in the latest Jurassic-earliest Cretaceous, the sedimentary succession comprising most of the GVF, the Great Valley Group (GVG), was deposited atop the Coast Range Ophiolite (CRO) and later, atop older GVG strata and the Franciscan subduction complex along the GVF's eastern margin. We apply U-Pb geochronology, zircon and whole rock geochemistry, and petrographic analyses to rocks of the GVG, Franciscan subduction complex, and CRO in the northern San Joaquin Basin to better understand the timing and tectonic location of initial forearc sedimentation, and how sediment routing systems may have evolved during Early to Late Cretaceous time. At Del Puerto Canyon, the oldest strata of the GVF basin are preserved as a series of black shales, with subordinate sandstone and limestone concretions, that accumulated during the earliest Cretaceous, between ~145-140 Ma. These strata, referred to as the Knoxville Formation, are separated by a ~40 myr unconformity with the overlying Upper Cretaceous deep-water turbidites of the Panoche Formation, which were deposited between ~96-85 Ma. Pre-Mesozoic age zircon grains are present in both the Knoxville and Panoche Formations, but sparse (0-7%) compared to other GVG sandstones. Zircon geochemical analyses support a predominantly felsic source (Th/U 0.9-0.2) during both periods of deposition, but Epsilon Hf signatures reveal a shift from contributions from juvenile to more evolved sources, broadly consistent with metavolcanic signatures of the Sierra Nevada magmatic arc, and more so with the Sierra Nevadan western metamorphic belt. Whole-rock geochemistry shows increasing compositional maturity from crystallization of the CRO during the latest Jurassic to deposition of the Knoxville and Panoche Formations during the Early and Late Cretaceous, respectively. Integrating these data, we present a tectonic model for the GVF basin at the latitude of Del Puerto Canyon that highlights the potential mechanisms to trap sediment during forearc initiation and hypothesize as to mechanisms to explain the ~40 myr unconformity and return to high-flux sedimentation during the earliest Late Cretaceous.

INTRODUCTION

Forearc basins are a common component of subduction margins and form along the oceanward side of volcanic arcs (e.g., Dickinson, 1973, 1974; Karig, 1974; Seely et al., 1974; Karig and Sharman, 1975). Forearc basin morphology varies significantly with the tectonics of specific margins. Therefore, forearc basins are categorized based on whether the margin is in a state of compression, extension, or neutrality, as well as whether the basin is along an accretionary or non-accretionary margin (e.g., von Huene and Scholl, 1991; Stern, 2002; Clift and Vannucchi, 2004; Noda, 2016). Forearc basins may transition amongst these end-member states as they respond to changes in subduction zone dynamics. Thus, the sedimentary record of ancient forearc basins provides a record of the tectonics of extant subduction zones. Whether a basin develops as a narrow (<50 km) and deep (>3 km) or wide (>50 km) and shallow (<3 km) basin or is a long- (>10 myr) or short-lived (<10 myr) feature, depends on the mechanisms that generate accommodation. Some of the working theories for forearc basin subsidence mechanisms include downward flexure from lithosphere load (Dickinson et al., 1995), activation of back thrust structures within an accretionary prism due to increased basal friction (e.g., Scholl et al., 1980; Larroque et al., 1995; Contardo et al., 2011), and reversal of surface slope angle (i.e., negative alpha basin) as seen in numerical modelling (Tharp, 1985; Byrne et al., 1993; Hassani et al., 1997; Mountney and Westbrook, 1997; Fuller et al., 2006; Bonnardot et al., 2008). Less commonly discussed are the effects of extension on basin subsidence, which may occur during basin formation (e.g., Trop et al., 2002; Stern, 2004; Orme and Surpless, 2019; Arukla et al. 2022) often coeval with or during a later-stage of lower-plate rollback.

The GVF basin in central California records sedimentation during latest Jurassic-earliest Cretaceous to Eocene oceanic subduction along the North American margin and is located between the Coast Ranges to the west and the Sierra Nevada and Klamath magmatic arcs to the east and north, respectively (e.g., Cowan and Bruhn, 1992; Dickinson, 1995; 2004). These three lithotectonic units represent the major components of the ancient subduction zone (Figure 1A). Along the western margin of the GVF basin, exposures of the Jurassic-Cretaceous Great Valley Group (GVG) form the eastern foothills of the Coast Ranges, which in turn are primarily composed of the ancient accretionary wedge known as the Franciscan subduction complex. Often separating rocks of the GVF basin and the Franciscan subduction complex are remnants of middle-late Jurassic ophiolitic material, collectively named the Coast Range Ophiolite (CRO). The Franciscan subduction zone complex, Jurassic and Cretaceous strata of the GVG, and its underlying basement, the CRO are present in the southern Great Valley Forearc, the San Joaquin Valley, at Del Puerto Canyon, California, ~35 km southeast of the city of San Jose (Figure 1B). This exposure at Del Puerto Canyon provides a unique opportunity to study the age, geochemical, and provenance relations amongst the three lithotectonic units, which in turn may eludicate the development of the GVF basin.

In this study, we integrate zircon U-Pb geochronology, zircon trace-element and Lu-Hf geochemistry, whole-rock geochemistry, and sandstone petrography to characterize the provenance and ages of GVG strata and Franciscan subduction complex exposures in Del Puerto Canyon, California. We also use petrography and geochemistry to determine the composition of the underlying CRO to interrogate the tectonic setting of its formation. Integration of these data from Del Puerto Canyon seeks to determine the coevolution of these distinct lithotectonic units,

leading to a clearer picture of the Jurassic-Cretaceous North American margin and the formation of the GVF basin.

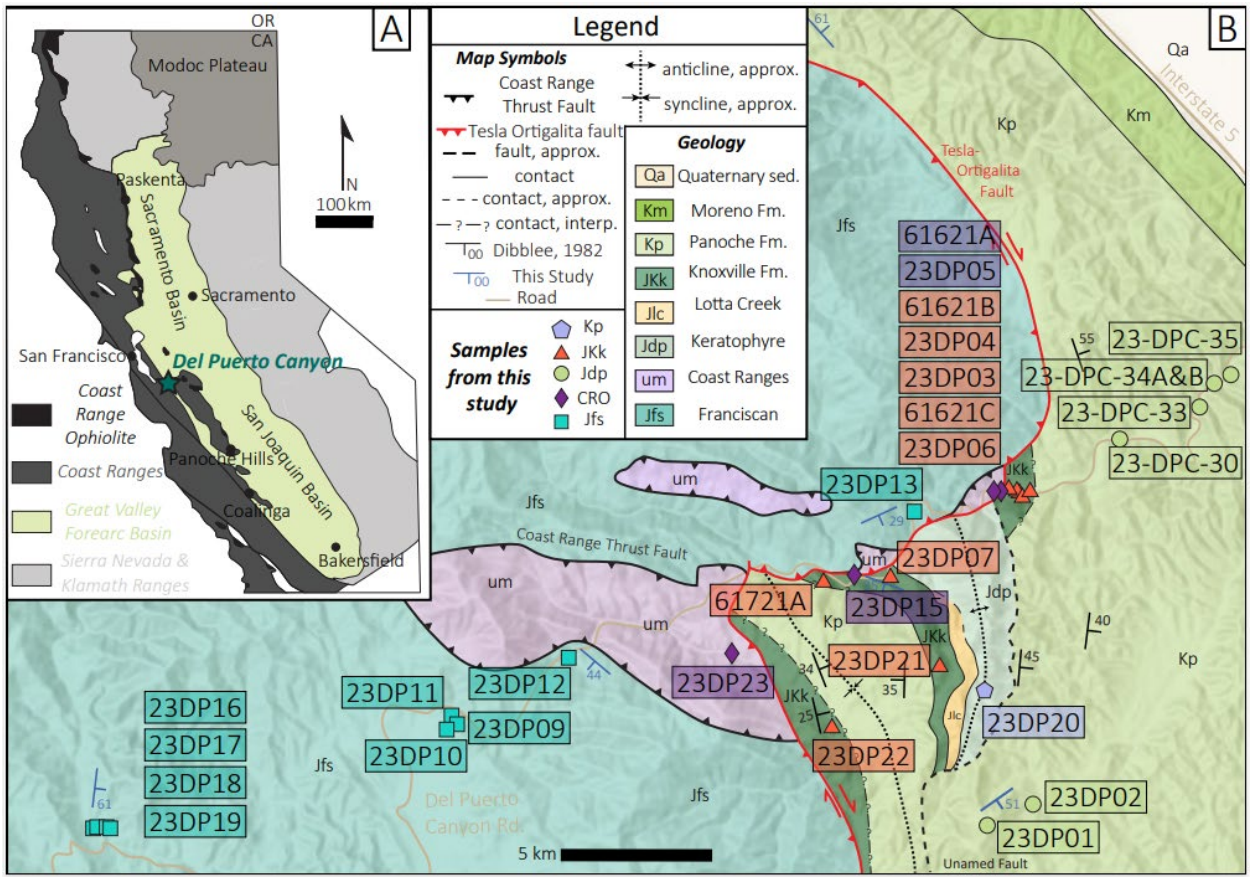

Figure 1. (A) Generalized geologic map of California highlighting the spatial extent of the Great Valley Forearc basin, modified from Orme and Graham (2018). (B) Revised geologic map of Del Puerto Canyon after Dibblee, 1982; 2007 and Maddock, 1964 and the results of this study. Stacked sample names are ordered from west to east, with the farthest west sample on top.

GEOLOGIC BACKGROUND

Jurassic-Cretaceous California Margin

The preservation of the Franciscan subduction complex and segments of the CRO within the Coast Ranges, the GVF basin, and magmatic arcs of the Sierran and Klamath mountains, provide a world-class natural laboratory for the study of ancient subduction dynamics. The Coast Ranges are primarily comprised of the Franciscan subduction complex, which is an assemblage of heterogeneous terranes characterized by varying metamorphic grades and lithologies that formed the accretionary wedge outboard of the GVF basin (Dickinson, 1981; Shervais et al., 2005; Hopson et al., 2008). While Franciscan-related subduction is interpreted to be active as early as ~180 Ma (Mulchay, 2018), the Franciscan wedge became accretionary at ~123 Ma (Dumitru et al., 2010; Apen et al., 2021) with the main stage of exhumation from ~100-70 Ma and continuing into the Cenozoic (Wakabayashi et al. 2010). Inboard and within exposures of the Franciscan complex, the Coast Ranges include remnants of ophiolitic material that comprise the CRO and form the basement to the GVF along its eastern margin. The crystallization ages of ophiolitic remnants in California vary from 169 to 155 Ma (see summary within Arkula et al., 2023). The tectonic setting in which the CRO remnants formed is debated and includes back-arc-inter-arc basin lithosphere (e.g., Moores, 1970; Schweickert and Cowan, 1975; Moores and Day, 1984; Ingersoll and Schweickert, 1986, and Ingersoll, 2019 and references therein), paleo equatorial mid-oceanic rift spreading center (Berger and Winterer, 1974; Evarts, 1977; Evarts and Schiffman, 1982; Robertson, 1989; Hopson et al., 1991; Hull et al., 1993; Hopson et al., 1996), and parautochtonous forearc lithosphere (e. g., Saleeby, 1982; Harper and Wright, 1984;

Shervais and Kimbrough, 1985; Wyld and Wright, 1988; Shervais, 1990; Saleeby and Busby-Spera, et al., 1992; Saleeby and Harper, 1993; Saleeby, 1996; Arkula et al., 2023).

The GVG consists of deep marine turbidites and shallow marine deposits, generally shoaling upward through time (e.g., Ojakangas, 1968; Ingersoll, 1978; Mansfield, 1979). The depositional age of the GVG was first determined through biostratigraphy, with the onset of sedimentation dated to Late Jurassic (Jones et al., 1969; Implay and Jones, 1970). The stratigraphically deepest GVG has also been dated using uranium and lead radioisotopes in detrital zircon which yield variable maximum depositional ages of ~151-135 Ma, thus indicating the beginning of the GVG deposition was diachronous during Late Jurassic to Early Cretaceous time (Orme and Surpless, 2019). The provenance of the latest Jurassic-earliest Cretaceous GVG is mainly within Jurassic volcanics of the Sierran-Kamath magmatic arcs and North American retroarc strata, whereas the Late Cretaceous GVG is primarily sourced from deeply eroded portions of the proximal magmatic arc (e. g., DeGraaff-Surpless et al., 2002; Sharman et al., 2015; Dumitru et al., 2015; Orme and Surpless, 2019; Surpless et al., 2019). Volcanic sources for the GVG were first identified through petrographic analysis of sandstone, conglomerate clast counts, and clay mineralogy (e.g., Ingersoll, 1979; Ingersoll, 1983). The petrofacies in the GVG contain metamorphic, plutonic, and volcanic arc detritus, thus recording eroded magmatic arc as a source for GVG (Ojakangas, 1968; Dickinson and Rich, 1972; Ingersoll, 1978, 1983; Mansfield, 1979). Petrographic analysis shows that the lower GVG is dominated by volcaniclastic and sedimentaclasic sandstones, whereas the upper GVG is dominated by plutoniclastic sandstones (Ingersoll, 1978). Detrital zircon studies that analyze the provenance of the GVG record a shift from generally unimodal age spectra to multipeak spectra, interpreted to

indicate changing source morphologies and sediment routing systems to the GVF (Degraaff-Surpless et al., 2002; Dumitru et al., 2010; Sharman et al., 2015). Trace element geochemistry reveals the source of much of the Cretaceous strata within the northern GVF (the Sacramento basin) and the southern GVF (the San Joaquin basin) to be between basaltic and andesitic composition, with significant sedimentary recycling (e.g., Cox et al., 1995; Surpless, 2014).

During the Early to Middle Jurassic Period, regions known today as the Sierra Foothills and Klamath Mountains accreted to the North American margin, after which the GVF developed (e. g., Schweickert and Cowan, 1975; Ingersoll and Schweickert, 1986; Ingersoll, 2000; Dickinson, 2008). Permo–Triassic to Cretaceous intra-arc strata of the Sierra Nevada reflect derivation from proximal arc activity, as well as the pre-Mesozoic sources from southwestern Laurentia (e.g., 1400–900 Ma, 500–300 Ma age peaks; Attia et al., 2021). During Late Jurassic-Eocene Franciscan subduction and coeval deformation, calc-alkaline plutons of the Sierran batholith were emplaced in the North American upper crust (e. g., Schweickert et al., 1984). There were magmatic high flux periods during Triassic (~250–190 Ma), Middle and Late Jurassic (~180–150 Ma), and mid-Cretaceous (~140–90 Ma) time, with each episode involving varying depths of pluton emplacement and magma addition rates (Paterson and Ducea, 2015).

Del Puerto Canyon, California

Del Puerto Canyon, located in the northern Diablo Range ~35 km southeast of San Jose, California, is part of the San Joaquin subbasin of the southern Great Valley forearc basin. Previous studies of Del Puerto Canyon have focused on detailed mapping and outcrop (E.g., Maddock, 1964; Dibblee, 1982; 2007) and petrologic descriptions of the CRO, with the latter exposed an almost complete ophiolite sequence (e.g., Evarts, 1977; 1978; 1992; Evarts et. al.,

1999). Pioneering mapping of the region by Dibblee (1982; 2007) included defining the Del Puerto Keratophyre and the Lotta Creek Tuff as part of the CRO, and work by Maddock (1964) further divided the GVG into the Jurassic Knoxville Formation, Albian Shale, Upper Cretaceous Panoche Formation, and overlying Moreno Formation (Anderson and Pack, 1915; Dibblee, 1982; 2007; Maddock, 1964; Bailey, 1970; Raymond, 1970; 1973) (Figure 1; Figure 2). There are two major fault systems in Del Puerto Canyon: the Coast Range Fault (CRF) and the Tesla-Ortigalita Fault (TOF) (e.g., Vickery, 1924; Briggs, 1953; Bailey 1970; Raymond, 1973) (Figure 1). The CRF is a thrust fault that superposed the GVG on top of the Franciscan Complex coeval with subduction and is often marked by serpentinite (e.g., Bailey, 1970; Raymond, 1973). The TOF is a normal and right-lateral strike-slip fault system comprised of high angle fault segments with various strikes that form an almost continuous boundary between the Franciscan and GVG or younger Cenozoic basin fill (Figure 1). The TOF cuts beds of the GVG including the Panoche Formation (Vickery, 1924; Huey, 1948; Raymond, 1973), and offsets segments of the CRF (Raymond, 1973; Figure 1). The oldest beds the TOF cuts are Lower Cretaceous in age, so the fault must have been active after this time, and in some areas, the TOF truncates Miocene beds, indicating reactivation of faulting in the Neogene because of potential Franciscan diapirism (Ernst, 1970; Huey, 1948; Raymond, 1973). The TOF is active today, evidenced by movement along the system during the 1983 Coalinga earthquake.

The Franciscan subduction complex in Del Puerto Canyon defines the western portion of the field area and consists of mostly sandstones and lesser components of greenstone, chert, and mélange (e.g. Raymond, 1973; Maddock, 1964; Dibblee, 1982; 2007). The sandstone portion is generally graywacke that is dark gray to gray, massive to bedded, fine grained, and interbedded

with siltstone or dark gray slaty shale (Maddock, 1964; Dibblee, 1982; 2007). Fossils indicate the Franciscan subduction complex in Del Puerto Canyon is ~152-145 Ma (Camp, 1942; Crittenden, 1951; Hall, 1958; Imlay, 1959; Maddock, 1964). The chert is thinly bedded, brittle, red, white, or green in color, and locally contorted (Dibblee, 1982; 2007). The greenstone (metabasalt) is black, massive, and locally brecciated, and it is often stained orange to red with iron and magnesium oxide (Maddock, 1964; Dibblee, 1982; 2007).

Thickness meters approx. scale	Lithology	Formation	Description	Depositional or Crystallization Age	Samples from this study *subsurface	TIMS	U-Pb	Hf-Lu	Petrog.	GC
6,400		Panoche Formation (Kp)	Massive, fine-medium grained, concretionary sandstone with calcareous or argillaceous matrix. Soft, gray, silty shale interbedded with thin, fine grained layers of sandstone, and coarse conglomerate. Adobe Flat Shale Member (Kpaf): Hard, dark gray to black silty shales. Gradational contact with the rest of the Panoche Formation. Concretions of gray, aphanitic limestone. Pea size conglomerate horizons mark unconformity between Kpaf and Jk. (Maddock, 1964; Anderson and Pack, 1915).	Turonian-Campanian 73-93 Ma (Bennison et al., 1991; Hosford Scheirer and Magoon, 2007)	23-DPC-35*		○			○
					23-DPC-34A*		○			
					23-DPC-34B*		○			
					23-DPC-33*		○	○		
					23-DPC-30*					○
					23DP02		○	○	○	○
					23DP01		○	○	○	
					23DP14		○		○	
1,500	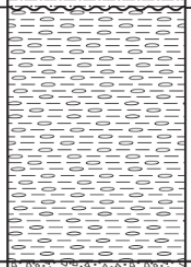	Knoxville Formation (Jk)	Dark gray to black clay shale with tuffaceous and radiolarian debris. Limestone concretions abundant near basal contact. Base Mg Ox sained red yellow chert along faulted base, could be gradational. (This Study)	Kimmeridgian-Berriasian 145 Ma (This Study)	23DP06		△	△	△	
					61621C		△		△	
					23DP03		△		△	
					23DP04G					△
					61621B		△		△	
					23DP07					△
					23DP21		△		△	
					61721A	△	△			
					23DP22	△	△		△	
270	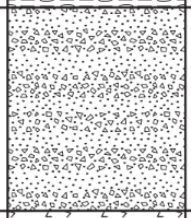	Lotta Creek Formation (Jlc)	Tuffaceous radiolarian chert with volcanic breccias, limited exposure of white crystaline tuffs (albite), lithics, and dark green shale. (Maddock, 1964).	Tithonian 150 Ma (Maddock, 1964)						
450	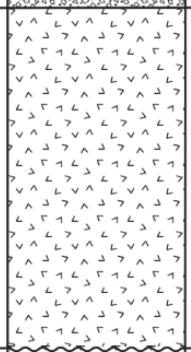	Del Puerto Keratophyre (Jdp)	Intermediate volcanic rock. Groundmass of chlorite, albite, quartz, and magnetite, with phenocrysts of mostly albite and minor quartz. Bounded by faults. (This Study; Maddock, 1964).	? Ma (This Study)	23DP20				⬠	
?	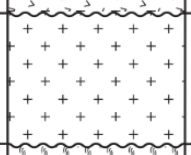	Coast Range Ophiolite (um)	Deformed and fragmented oceanic meta-igneous and igneous assemblages. Gabbroic dikes, serpentinized volcanics, basalts, chert. (Bailey et al., 1970)	Oxfordian 158 & 160 Ma (Lanphere, 1971)	61621A					◊
					23DP05				◊	◊
					23DP15				◊	
					23DP23				◊	
2,400-6,000 not well documented in Del Puerto Canyon	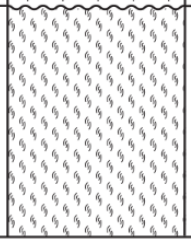	Franciscan (Jfs)	Massive, medium grained sandstone in the upper 4,500 m of the section. Thin bedded, fine grained gray sandstone, interbedded with dark gray slaty shale in the lower 1,500 m of the section. (Maddock, 1964).	Callovian to Berriasian 145-164 Ma (Maddock, 1964)	23DP13				□	
					23DP12		□	□	□	
					23DP09				□	
					23DP11		□		□	
					23DP10				□	
					23DP19				□	
					23DP18				□	
					23DP17		□		□	
					23DP16		□		□	

Figure 2. Pseudo-tectonic stratigraphic column of Del Puerto Canyon, including sample names and analytical data type for this study. All thickness data is from the same reference as the description (Anderson and Pack, 1915; Maddock, 1964; Bailey et al., 1970; Lanphere, 1971; Evarts, 1977; Dibblee, 1982; 2007). The upper age of the Panoche Formation at Del Puerto Canyon is reported as old as ~93 Ma from biostratigraphy (Bennison, 1991) and maximum depositional ages from this study, but within the subsurface to the south is reported as young as ~83.5 Ma (Hosford Scheier and Magoon, 2007).

The CRO in Del Puerto Canyon is present as deformed and fragmented oceanic meta-igneous and igneous assemblages, which includes gabbroic dikes, serpentinized volcanics, basalt, and chert (Bailey et al., 1970). The crystallization ages from the CRO are between 161-155 Ma, recorded by U-Pb in zircon and Ar-Ar in Hornblende found in plagiogranite veins in quartz diorite and tonalite (Lanphere, 1971; Hopson et al., 1981; Evarts, 1992; Mattinson et al., 2008). A series of dikes that cut the cumulates and a rhyolite at the top of the volcanic portion of the ophiolitic succession yield dates between ~150-149 Ma (Evarts, 1992). The Del Puerto Keratophyre is a mappable unit, interpreted as the upper volcanic section of the CRO as first defined by Dibblee (1982; 2007) and described by Evarts (1992) and consists of intermediate volcanic rock that has a groundmass of chlorite, albite, quartz, and magnetite, with phenocrysts including albite and minor quartz (this Study; Dibble, 1982; 2007; Maddock, 1964). The Keratophyre is bounded by the TOF to the north and an unnamed fault to the east, and is deformed into an anticline (Maddock, 1964; Raymond, 1973; Dibblee, 1982; 2007).

The Lotta Creek Formation is stratigraphically above the Del Puerto Keratophyre and crops out south of the main canyon (Figure 1B). The volcanic formation is comprised of tuffaceous radiolarian chert with volcanic breccias, limited exposure of white crystalline tuffs (albite), white tuffaceous sandstone, lithics, and dark green shale (Maddock, 1964; Raymond,

1970, 1973: Dibblee, 1982; 2007). An andesite boulder within the formation dates to ~150 Ma (Ar-Ar on hornblende: Evarts, 1992).

The Knoxville Formation conformably and gradationally overlies the Lotta Creek Formation (Figure 1B) and contains dark gray, black, and purple clay shales with gray limestone concretions near the basal contact containing fossils, and thinly bedded sandstone layers interbedded with the shales (Cittenden, 1951; Hall, 1958; Maddock, 1964). The Knoxville Formation is classically assigned a latest Jurassic depositional age and is the most basal member of the GVG within the San Joaquin basin (e.g., Cittenden, 1951; Hall, 1958; Maddock, 1964).

The Panoche Formation unconformably overlies the Knoxville Formation and makes up most of the GVG strata mapped in Del Puerto Canyon (Anderson and Pack, 1915; Maddock, 1964; Dibblee, 1982; 2007). A thin, pea-size conglomerate horizon marks the unconformity between Knoxville and Panoche (Anderson and Pack, 1915; Maddock, 1964). The lower Turonian Adobe Flat Shale Member forms the base of the Panoche Formation, and is a hard, dark gray to black silty shale that grades into overlying sandstones (Maddock, 1964). In places along Del Puerto Creek, the presence of limestone lenses and concretions between shale layers is what led authors to group these shales as the Adobe Flat Shale Member. By contrast, the bulk facies found within the Panoche Formation consist of massive, fine to medium grained-sandstone with argillaceous or calcareous matrix interbedded with soft, brown to gray, silty shale (Anderson and Pack, 1915; Maddock, 1964). The Panoche Formation has been dated using fossils and U-Pb maximum depositional ages (MDAs) from detrital zircons to be ~87-93 Ma (Maddock, 1964; Sharman et al., 2015; this Study).

The Moreno Formation is present in the northeast corner of this field area and is comprised of brown clay shale that has limestone concretions and interbedded massive gray sandstone (Anderson and Pack, 1915; Maddock, 1964; Raymond, 1970; Bishop, 1970). It overlies the Panoche Formation with gradational depositional contact, and in this field area, only the lower portion of the formation is visible (Maddock, 1964). The presence of foraminifera, ammonites, and reptile remains indicate that the Moreno Formation was deposited in the latest Late Cretaceous in a marine environment (Maddock, 1964).

METHODS

Field Geology and Core Repository

At each field site, we took GPS coordinates, examined contacts, conducted a detailed lithofacies description, and used a Brunton Compass to measure strike and dip of bedding. We were unable to complete measured stratigraphic sections or detailed mapping beyond single field stations due to limited access to private property. At many field stations, we collected samples for detrital U-Pb geochronology (N = 18), Lu-Hf geochemistry (N=5), sandstone petrography (N = 8), igneous and/or metamorphic petrology (N = 12) and whole rock geochemistry (N= 5) (Figure 1B; Figure 2).

Given our limited access to the field area mapped as the Panoche Formation, we collected subsurface sandstone samples for U-Pb geochronology (N=4), Lu-Hf (N=1), and whole rock geochemistry (N=2) from the California Core Repository in Bakersfield, CA (Figure 2). Open access drilling reports and well logs with gamma and sonic ray curves were used to identify sandstone intervals in core sections. To ensure enough zircon yield for detrital analyses, each sample is a composite from core chippings from -91 and -293 meters below the Kelly Bushing datum (Appendix A; Figure 1B). We ensured that all of the chippings samples we collected were consistently medium-grained sandstone and did not exhibit any changes in bulk mineralogy with depth.

Geochronology

U-Pb geochronology was completed for detrital zircons from eighteen sandstone samples to determine provenance and maximum depositional ages of sedimentary rocks (Williams, 1997;

Gehrels, 2012). Samples include nine medium-grained sandstones from mapped outcrops or subsurface wells of the Panoche Formation, one-medium grained sandstone from mapped Knoxville Formation, four medium-grained sandstones at the eastern-most contact with the CRO that are either mapped as Knoxville Formation, Albian Shale, or lower Turonian Adobe Flat Shale member of the Panoche Formation (Maddock, 1964; Bishop, 1970; Dibblee, 1982; 2007), and four medium to coarse-grained sandstones from the Franciscan subduction complex. Mineral separation for zircon was completed using standard heavy mineral separation techniques (e.g., Gehrels et al., 2008). We used backscattered electron (BSE) images to randomly select 315 detrital zircon grains without significant inclusions or cracks.

In this study, we analyzed our zircons with laser ablation inductively coupled plasma mass spectrometry (LA-ICP-MS) at the University of Arizona Laserchron Center using a Thermo Element2 single collector ICP-MS. U-Pb analyses were conducted with a 20 μm spot diameter, resulting in a 12 μm pit depth on each evaluated grain. U-Pb data were filtered to exclude ages with high common Pb, >5% reverse discordance, >10% uncertainty, or >20% discordance. The reported ages are based on the $^{206}Pb/^{238}U$ ages for grains < ~1.0 Ga and on the $^{206}Pb/^{207}Pb$ ages for grains > ~1.0 Ga (Gehrels et al., 2008; Gehrels, 2012). Th/U ratios measured during this analysis were used for zircon trace element geochemical analysis. All data were reduced using *AgeCalcML,* a Matlab-based graphical user interface (GUI) that is used for reducing, visualizing, and reporting data collected by LA-ICP-MS (Sundell et al., 2020). U-Pb data are reported in Appendix B.

Two sandstones (61721A and 23DP22) analyzed for U-Pb geochronology with LA-ICP-MS were further interrogated with CA-ID-TIMS (chemical abrasion isotope dilution thermal

ionization mass spectrometry). CA-ID-TIMS provides a more precise age than LA-ICP-MS, therefore allowing for closer inspection of outlier grains, such as a young tail of single ages that do not overlap the bulk of analyses. CA-ID-TIMS was performed at Boise State University following the protocols modified after Mattinson (2005). Cathodoluminescence (CL) images were obtained with a Hitachi TM4000Plus scanning electron microscope. Grains selected for TIMS analysis based on CL images and LA-ICPMS data were removed from the mounts and annealed at 900°C for 60 hours in a muffle furnace. Zircon was dissolved and rinsed in multiple stages of HF, HNO_3, ultrapure H_2O, and HCl, and then spiked with the Boise State University mixed ^{233}U-^{235}U-^{205}Pb tracer solution (BSU-1B). U and Pb were separated from the zircon matrix using an HCl-based anion-exchange chromatographic procedure (Krogh, 1973), eluted together and dried with 2 µl of 0.05 N H_3PO_4. Pb and U were loaded on a single outgassed Re filament in 5 µl of a silica-gel/phosphoric acid mixture (Gerstenberger and Haase, 1997), and U and Pb isotopic measurements made on a GV Isoprobe-T multicollector thermal ionization mass spectrometer equipped with an ion-counting Daly detector. Pb isotopes were measured by peak-jumping all isotopes on the Daly detector for 160-200. U mass fractionation was corrected using the known $^{233}U/^{235}U$ ratio of the Boise State University tracer solution. CA-ID-TIMS U-Pb dates and uncertainties were calculated using the algorithms of Schmitz and Schoene (2007), U decay constants recommended by Jaffey et al. (1971), and $^{238}U/^{235}U$ of 137.818 (Hiess et al., 2012). We corrected $^{206}Pb/^{238}U$ ratios and dates for initial ^{230}Th disequilibrium using $D_{Th/U} = 0.20 \pm 0.05$ (1s) and the algorithms of Crowley et al. (2007). All common Pb in analyses was attributed to laboratory blank and subtracted based on the measured laboratory Pb isotopic composition and associated uncertainty.

Provenance

The complete distribution of detrital zircon ages within a sample can help characterize source terranes and provide information on the tectonic setting of strata (e.g., Cawood et al., 2012; Gehrels, 2012; 2014). AgeCalcML was used to construct a series of vertically stacked histograms and kernel density estimates (KDEs) to visually compare age spectra from multiple samples (Gehrels et al., 2008; Horstwood et al., 2016; Sundell et al., 2020). KDEs display the continuous probability of the age distribution of a sample, but do not incorporate uncertainties since the Gaussian kernel bandwidth can be set by the user to optimize data visualization based on the distribution of ages (Sundell et al., 2020). In AgeCalcML (Sundell et al., 2020) we set bin width for all ages to 50 M.y., kernel bandwidth for 50-250 Ma grains to 5 M.y., and kernel bandwidth for grains older than 250 Ma to 20 M.y.

Maximum Depositional Ages

The youngest component of a sedimentary rock can be used to constrain its maximum depositional age (MDA), which may approximate the true depositional age (TDA) in convergent tectonic settings with active arcs and young zircon grains (e.g., Dickinson and Gehrels, 2009; Cawood et al., 2012; Spencer et al., 2016; Coutts et al., 2019; Herriott et al., 2019). There are a range of statistical methods used to determine the MDA, including the youngest single zircon grain (YSG), youngest cluster of at least three grains whose errors overlap within two sigma uncertainty (YGC2σ 3+), and youngest statistical population (YSP) (e. g., Gehrels, 2003; Dickinson and Gehrels, 2009; Coutts et al., 2019). YSP is a weighted average of the youngest group of two or more grains that have a mean square weighted deviation (MSWD) of ~1.00 (Coutts et al., 2019). We use the Matlab based program *DZMda* to calculate YSG, YSP, and

YGC2σ3+ (Sundell et al., 2024). In addition, we consider the maximum likelihood age (MLA), which we calculate using *IsoplotR* Online (Galbraith, 1988; Galbraith and Laslett, 1993; Vermeesch, 2018; 2021).

We report the age of the youngest single grain from each sample, with no filtering. However, prior to calculating YSP, YGC2σ3+, and MLA, we examined the youngest series of dates and did not include in MDA calculations any grains that did not overlap with another grain within 2-sigma error because these skew the data to erroneously young dates that use fewer than 2 grains to calculate an MDA. We report a range of MDA calculations to highlight differences in the resulting MDA based on each method, but we use the YSP date as the best estimate TDA in Del Puerto Canyon following Herriott et al. (2019). YSG and YGC2σ3+ often record MDAs that are too young and can routinely underestimate MDAs, whereas YSP calculations are more conservative and are less likely to capture erroneously young grains or tails that could have been affected by Pb loss (Herriott et al., 2019). For two samples with a scattering of young dates that do not overlap the youngest age population, we use weighted mean calculations of the youngest subset of grains that were analyzed using CA-ID-TIMS.

Petrography

Twenty-one rock samples from Del Puerto Canyon were collected, cut, and stained for Ca-plagioclase and K-feldspar as standard petrographic thin sections. Nine are sandstones from GVG strata, and the remainder are igneous, metamorphic, and sandstone samples from the CRO and Franciscan subduction complex (Figure 1 and 2). The composition and provenance of the GVG samples were analyzed by counting three-hundred framework grains according to the Gazzi-Dickinson point-counting method (Gazzi, 1966; Dickinson, 1985), with only samples

comprised of less than 15% matrix analyzed. In addition to the 300 framework grains, we recorded the composition of the matrix and cement, and took note of any sedimentary structures and textures to gain insight into the depositional and post-depositional environment of the sedimentary samples. Point counting data, including grain types and modal parameters for all twenty-four samples, are available in Supplementary Material.

The mineralogy of the CRO and Franciscan samples was also analyzed by documenting the primary groundmass and minerals present. When samples consisted of distinct framework minerals, three-hundred framework grains were counted according to the Gazzi-Dickinson point-counting method (Gazzi, 1966; Dickinson, 1985). We recorded any igneous textures and metamorphic fabrics for these samples to determine the origin and extent of metamorphism and deformation, respectively.

Lu-Hf Geochemistry

Lutetium-Hafnium (Lu-Hf) isotopic ratios, reported as epsilon hafnium (εHf) values, can be combined with U-Pb age data to give insight on the type of magma from which zircon crystallized (Vervoort, 2014). The εHf values are categorized as evolved (negative εHf) or juvenile (positive εHf), in comparison to CHUR (chondritic uniform reservoir). Evolved signatures imply the zircon was crystallized from evolved arc magmas, often intruding older continental material, whereas juvenile signatures support crystallization from undifferentiated, more mafic magma sources (e.g., Hofmann, 1997; Vervoort, 2014). We analyzed five samples for Lu-Hf after U-Pb analysis at Arizona Laserchron Center, using the practices outlined by Gehrels and Pecha (2014) and Ibanez-Mejia et al. (2014). We chose grains from the two primary zircon age populations found in GVG strata (160-140 Ma and 100-90 Ma), and we selected

grains that would fit a 40-micron laser spot in addition to the 15-micron U-Pb analysis spot. After data reduction in *AgeCalcML* (Sundell, 2021), εHf values are plotted as individual points overlain on heat maps to distinguish between different units in the field area.

Whole Rock Trace Element Geochemistry

Seven samples from Del Puerto Canyon were analyzed for trace element concentrations using ICP-MS and loss on ignition (LOI) at Washington State University following routine methods of Knaack et al. (1994) and Johnson et al. (1999). Samples were collected from specific units as mapped by Dibblee (1982; 2007) and Maddock (1964), with two mudstones within the Knoxville Formation, three mudstones within the Panoche Formation, and two igneous samples within the CRO (Figure 2). Analyzing the trace element geochemistry of the sedimentary samples can distinguish mafic components, source region, and degree of weathering and recycling of sediments (McLennan et al., 1993; Fralick, 2003; Surpless, 2014). The trace element geochemistry of the igneous samples is used to gain insight into the type of magma from which the rocks crystallized from, and therefore infer their tectonic setting (Hoffman, 1970). Mantle convection leads to a globally heterogeneous mix of magma composition; as a melt separates from the mantle, elements that are incompatible (e.g., U, Th, K) migrate to other regions (Hofmann, 1970). Because of their varying tectonic settings and therefore mantle interactions, mid ocean ridge basalt (MORB), ocean island basalt (OIB), and igneous units that have interacted with continental crust or evolved mantle will have varying chemical signatures, both isotopically and within their trace element compositions (Hofmann, 1970).

In sedimentary geochemistry, trace elements help determine provenance because they are generally excluded from seawater and have low post-depositional mobility (McLennan et al.,

1993). In mafic sedimentary rocks, such as shale and mudstone, immobile trace elements such as Th, Sc, and La help determine provenance and composition (Armstrong-Altrin and Verma, 2005; Ryan and Williams, 2007). To ascertain if the sediment's crustal source was more evolved or juvenile, we can plot the samples La, Th, and Sc values in a ternary diagram (Bhatia and Crook, 1986; McLennan et al., 1990, 1993; Surpless 2014). Juvenile, MORB, crustal components plot towards the Sc corner of the diagram, whereas more evolved, NASC and UCC continental crustal components, plot closer towards the La corner of the plot in a linear trend. Using these trace elements, we can estimate the composition and source of the rocks and the processes that occurred to generate the geochemical composition of our sediments: magmatic differentiation and/or sedimentary recycling. In addition, a Zr/Sc vs Th/Sc plot, is used to compare our samples to what we would expect from MORB, andesite, and upper crust (granodiorite); as Zr/Sc ratio increases, we expect an increase in sedimentary recycling, and as Th/Sc increases, we see an increase in magmatic differentiation.

RESULTS

U-Pb Age Spectra

Samples collected from the GVG predominantly consist of Mesozoic age grains, with <2% pre-Mesozoic dates, and fall into two groups (Figure 3). Seven samples (23DP22, 61721A, 23DP21, 61621B, 23DP03, 61621C, 23DP06) consist of a unimodal age distribution centered at ~145 Ma with zero to six pre-Mesozoic grains in each sample (Figure 3; middle panel). Sample 23DP21 was collected within strata mapped by Dibblee (1982; 2007) and Maddock (1964) as the Knoxville Formation, 23DP22 and 61721A were collected from mapped Panoche Formation, and samples 61621B, 23DP03, 61521C, and 23DP06 were collected moving progressively east from the contact with the keratophyre (Figure 1B). Six samples from mapped or subsurface Panoche Formation (23DP01, 23DP02, 23-DPC-33, 23-DPC-34B, 23-DPC-34A, 23-DPC-35) consistently show a bimodal age spectrum with peaks at ~89-93 Ma and ~145 Ma (Figure 3, top panel); these samples contain two to twenty-one pre-Mesozoic grains per sample (Figure 3). The four sandstones collected from the Franciscan subduction complex (23DP16, 23DP17, 23DP11, 23DP12) show a multimodal age spectrum with variable Mesozoic age peaks between 250-80 Ma (Figure 3) and 6-52% pre-Mesozoic grains. Pre-Mesozoic age grains for three of the four (23DP11, 23DP12, 23DP17) Franciscan samples show peaks, of various magnitudes, ranging between ~250-450 Ma, ~1000-1200 Ma, ~1400-1600, ~1600-1800, and a few >2000 Ma grains. Sample 23DP16, differs from other Franciscan samples in the field area, as it contains major age populations between 1330-1470 Ma and ~1600-1800 Ma, and lacks the ~250-450 Ma grains.

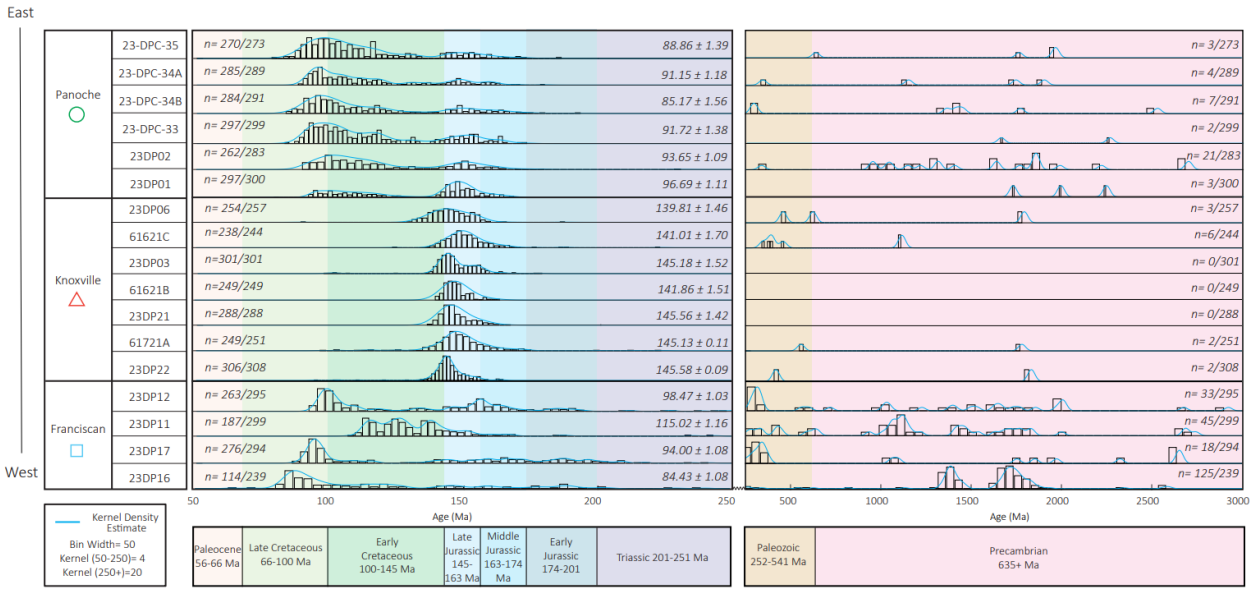

Figure 3. Detrital zircon kernel density estimates (KDEs) of 17 sandstones from Del Puerto Canyon stacked from east (top) to west and grouped by geologic formation. Mesozoic KDEs (50-250 Ma) are normalized to each other, with the reported maximum depositional age (MDA) of each sample (see Table 1 and Figure 4 for additional MDA details). Following a break in scale, Paleozoic and Precambrian (251-3000 Ma) KDEs are normalized to each other and highlight the lack of these age grains within Great Valley Group sandstones at Del Puerto Canyon.

Maximum Depositional Ages

The seven sandstones with a unimodal age spectra yield YSP MDAs of ~139-145 Ma, with other MDA methods generally overlapping this range (Figure 4). Initial LA-ICP-MS analyses on samples 61721A and 23DP22 yielded a young tail of scattered dates (n= 7) that do not overlap the unimodal age spectra centered at ~145 Ma. Therefore, we performed CA-ID-TIMS on a subset of these grains to test for the accuracy of LA-ICP-MS dates and the potential effects of Pb loss leading to erroneously young dates. Sample 61721A yields six CA-ID-TIMS dates: 145.14 ± 0.12, 145.10 ± 0.32, 117.32 ± 0.11, 111.86 ± 0.08, 101.55 ± 0.11, and 95.18 ± 0.15. The two oldest dates (~145 Ma) are significantly older than their LA-ICP-MS dates of ~125 and ~124 Ma, respectively, suggesting Pb loss may have affected LA-ICP-MS dates (Table

1). In contrast, three other dates overlap LA-ICP-MS dates, and one is a bit younger. We choose to use the oldest two dates that overlap within 1-sigma error to calculate a weighted mean of 145.10 ± 0.22, which we report as the MDA for this sample. We do not choose to include the other CA-ID-TIMS dates in any MDA calculation as they do not overlap within error of each other. Sample 23DP22 yields six CA-ID-TIMS dates: 146.19 ± 0.22, 145.90 ± 0.19, 145.30 ± 0.11, 128.09 ± 0.09, 123.11 ± 0.17, and 115.56 ± 0.31. From these six dates, the oldest three overlap within 1-sigma error and yield a weighted mean of 145.60 ± 0.17, which we report as the MDA for this sample. The youngest TIMS dates are excluded from the weighted mean MDA calculation because the grains are more dispersed, with 5-10 Ma between them and lack of correlation with ages of strata in the field area. Although we use the weighted mean for interpretation of MDA for samples 61721A and 23DP22, the implication of all TIMS dates and LA-ICP-MS MDA calculations for each sample will be discussed further and are included in Figure 4.

Panoche sandstone samples yield YSP MDA's of ~ 97-85 Ma, and all other MDA methods overlap the YSP within error (Figure 4). Three sandstones (23DP16, 23DP17, 23DP12) from the Franciscan subduction complex yield YSP MDAs of ~98-84 Ma, with other MDA methods overlapping within error (Figure 4). In contrast, sample 23DP11 yields a YSP MDA of 115.02 ± 1.16, which overlaps the MLA of 115.82 ± 1.35 (Figure 4).

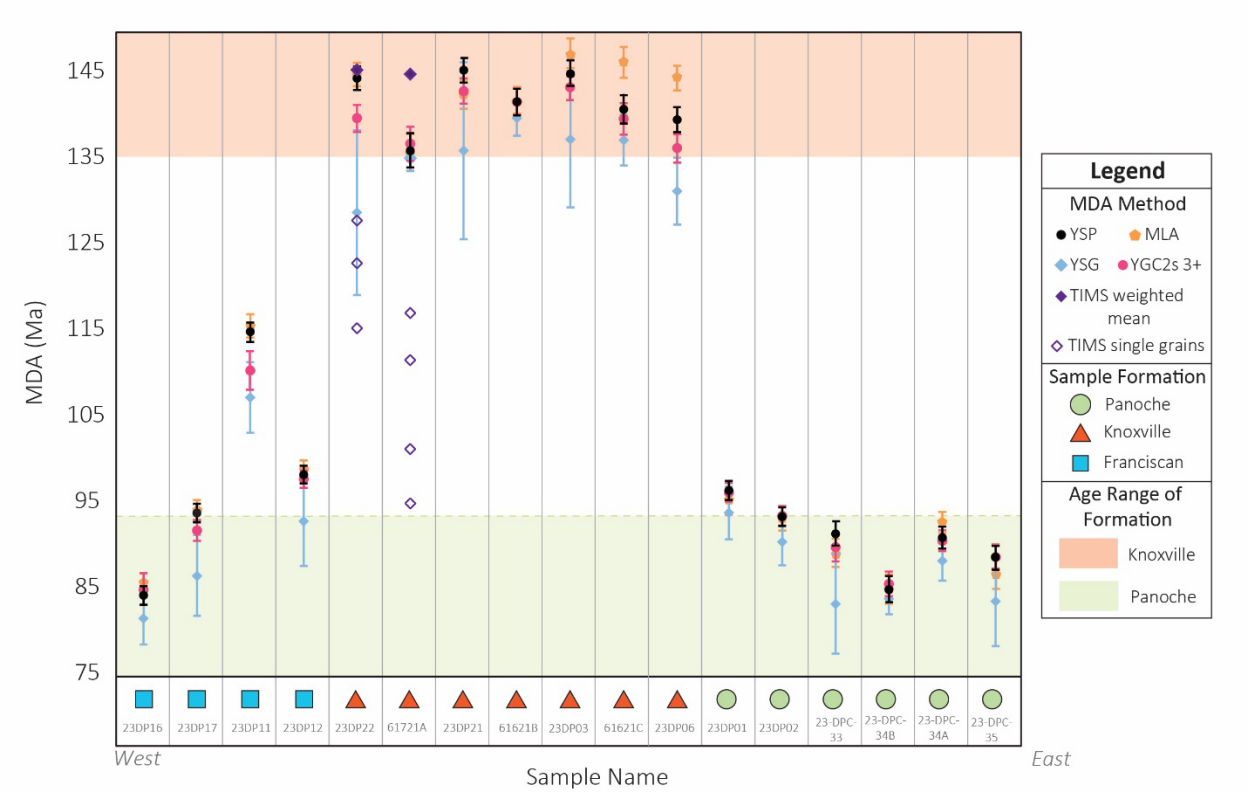

Figure 4. Maximum Depositional Ages for all 17 samples shown in Figure 3 calculated using methods described in the text including youngest statistical peak (YSP), maximum likelihood age (MLA), youngest single grain (YSG), youngest cluster of three or more grains with overlapping error of 2 sigma (YGC2s 3+), TIMS weighted mean. MLA and weighted means calculated with IsoplotR (Vermeesch, 2014); all other methods calculated with DZmda (Sundell, 2020). CA-ID-TIMS grains shown as open purple diamonds did not overlap with uncertainties with other dates and therefore were not used for the weighted mean calculations (See discussion for more details).

Sample Name	ALC LA-ICPMS Spot Label	206Pb /238U Date (Ma)	± (1-sigma)	Resulting Unit Assignment based on TIMS alone	ALC U-Pb LA-ICP-MS Best Age	U-Pb LA-ICP-MS Error	Final Unit Assignment
61721A	**251**	**145.1**	**0.1**	**Knoxville Formation**	**125.9**	**1.5**	
61721A	**75**	**145.1**	**0.3**	**Knoxville Formation**	**124.5**	**2.7**	
61721A	96	117.3	0.1	Albian Shale	115.6	1.9	Knoxville Formation
61721A	158	111.9	0.1	Albian Shale	110.9	1.3	
61721A	12	101.6	0.1	Albian Shale	103.9	1.6	
61721A	271	95.2	0.2	Albian Shale	103.1	1.4	
23DP22	**227**	**146.2**	**0.2**	**Knoxville Formation**	**133.9**	**9.2**	
23DP22	**109**	**145.9**	**0.2**	**Knoxville Formation**	**102.6**	**3.5**	
23DP22	**188**	**145.3**	**0.1**	**Knoxville Formation**	**94.7**	**3.2**	Knoxville Formation
23DP22	266	128.1	0.1	unknown ?	129.0	9.6	
23DP22	193	123.1	0.2	unknown ?	121.0	5.7	
23DP22	180	115.6	0.3	Albian Shale	111.3	4.7	

Table 1. CA-ID-TIMS comparison and classification. LA-ICP-MS and CA-ID-TIMS U-Pb ages from grains within samples 23-DP-22 and 61721A are reported and used to classify each sample by age into the Knoxville Formation.

Petrography

The average composition of eight samples of GVG strata from Del Puerto Canyon are 33% quartz, 32% feldspars, and 35% lithics (Figure 5, Appendix D). Ninety-five percent of the quartz is monocrystalline (Qm) and the remainder is polycrystalline (Qp). Among the feldspar grains, 50% are plagioclase feldspar (P) and 50% are potassium feldspar (K). Lithics are primarily volcanic, with lathwork (17%), granulitic (55%), and microlitic (28%) textures. Notably, Knoxville samples have a total of 161 detrital olivine (O) present, and olivine comprises 3-14% of the framework grains of each sample (Figure 5, Appendix D). Both Knoxville and Panoche samples have accessory detrital minerals including muscovite, biotite, calcite, and chlorite. All GVG samples lack evidence of deformation, contain minor plagioclase replacement by calcite, and generally contain cement and matrix comprised of micas, iron oxides, and calcite (Figure 5A-E).

The composition and texture of the Del Puerto Keratophyre and CRO samples are shown in representative thin section photos (Figure 6A-E). Del Puerto Keratophyre (23DP20), shows

polycrystalline quartz with lathwork volcanics and minor calcite (Ca) (Figure 6A). From the CRO, sample 23DP05 is mostly lathwork volcanics and plagioclase feldspar, and it contains veins of calcite and polycrystalline quartz (Figure 6B). Sample 23DP23 is comprised of clinopyroxene, serpentine, lizardite, olivine, and contains microfractures within the grains (Figure 6C). Sample 23DP15B shows lizardite and corona texture with mostly clinopyroxene (Cpx), orthopyroxene (Opx), and serpentine (S) (Figure 6D-E).

The variation of texture and composition of Franciscan subduction complex samples in Del Puerto Canyon is shown in representative thin section photos (Figure 6F-H). Sample 23DP10 is a serpentinite and has minor iron oxide staining (Figure 6F). By contrast, samples 23DP16 and 23DP17, show framework grains comprised of monocrystalline quartz, polycrystalline quartz, plagioclase feldspar, potassium feldspar, and accessory detrital serpentinite (Figure 6G-H).

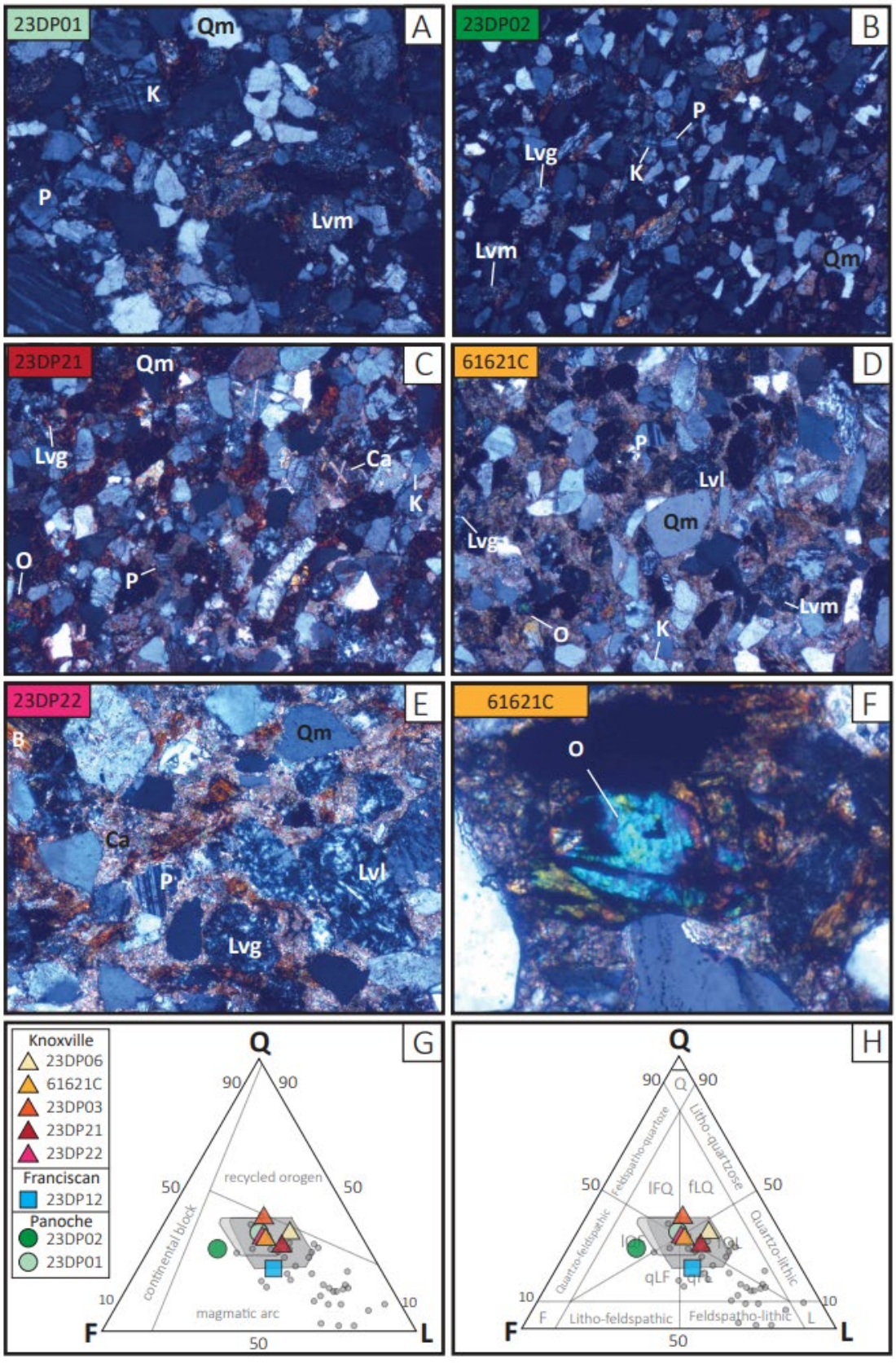
23DP01
A
Qm
K
P
Lvm
23DP02
B
P
Lvg
K
Lvm
Qm
23DP21
C
Qm
Lvg
Ca
K
O
P
61621C
D
P
Lvl
Qm
Lvg
Lvm
O
K
23DP22
E
Qm
Ca
P
Lvl
Lvg
61621C
F
O
Knoxville
23DP06
61621C
23DP03
23DP21
23DP22
Franciscan
23DP12
Panoche
23DP02
23DP01
G
Q
90
90
50
50
recycled orogen
continental block
magmatic arc
10
10
F
50
L
H
Q
90
90
Q
50
50
Feldspatho-quartose
Litho-quartzose
lFQ
fLQ
Quartzo-feldspathic
Quartzo-lithic
lQL
qLF
qFL
10
10
F
Litho-feldspathic
Feldspatho-lithic
L
50
F
L

Figure 5. Panels A-F: Characteristic thin section images from GVG strata in Del Puerto Canyon. Magnification for panels A-E is 4x, and the scale bar in the top left corner in 400 microns and contains the sample name. The magnification of panel F is 10x, and the scale bar is 100 microns long. Images were all taken under cross polarized light (XPL). Bt: biotite, Pl: plagioclase, Lvm: volcanic, microlitic, Lvl: volcanic, lathwork, Lvg: volcanic, felsitic, granular, Ca: calcite, Qp: polycrystalline quartz, Qm: monocrystalline quartz, O: Olivine. Panel G: Ternary diagram with abundance of total quartz (Q), total feldspar (F), and total lithics (L), classified by provenance. Panel H: Ternary diagram with abundance of total quartz (Q), total feldspar (F), and total lithics (L), classified by rock type. Panels G and H reference data from Dickinson and Rich (1972) and references therein, Romero et al. (2024), and fields of SJV and Sacramento basin from Surpless (2014) adapted from Ingersoll (1983).

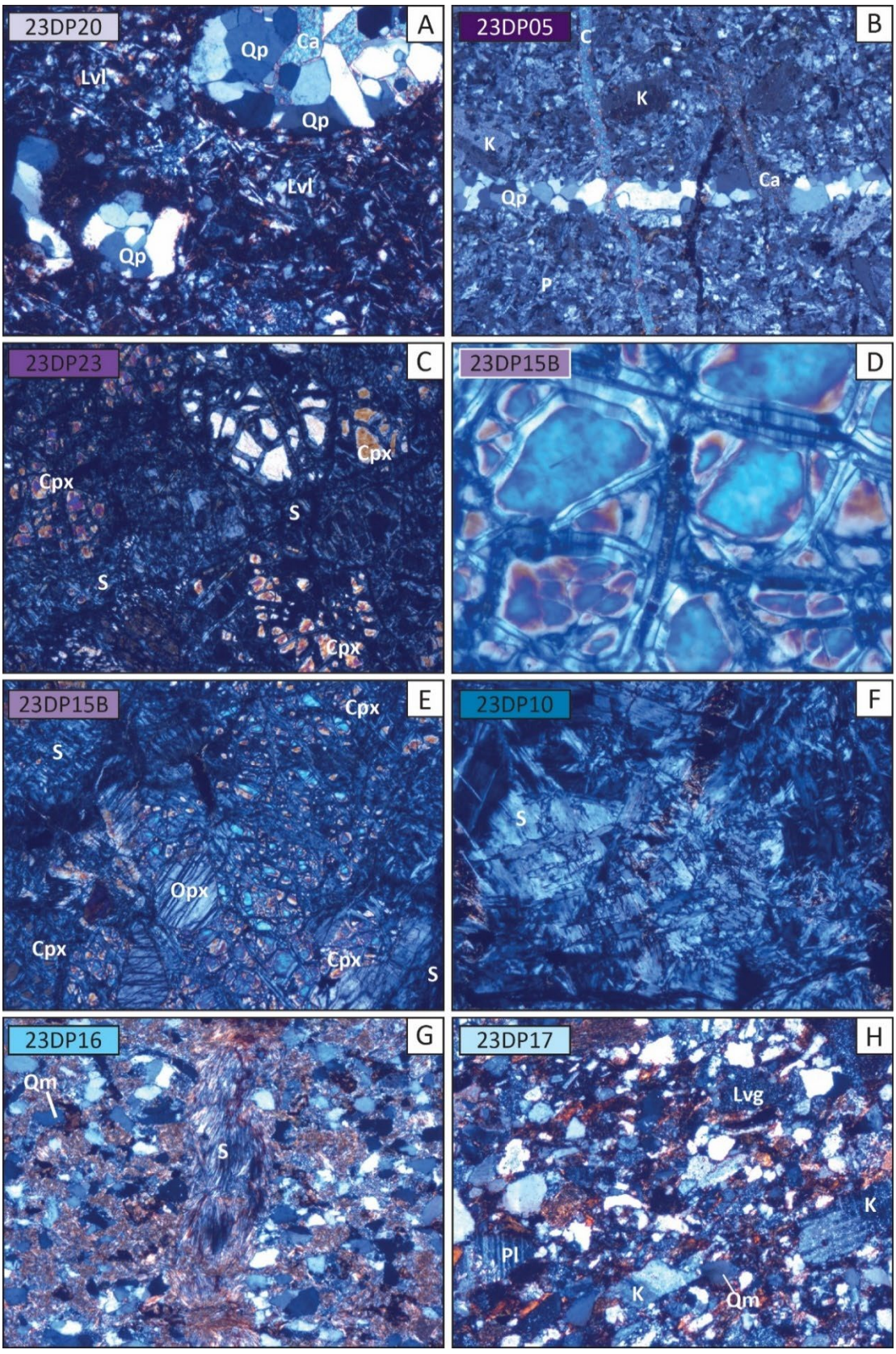
23DP20
A
Qp
Ca
Lvl
Qp
Lvl
Qp
23DP05
B
C
K
K
Ca
Qp
P
23DP23
C
Cpx
Cpx
S
S
Cpx
23DP15B
D
23DP15B
E
Cpx
S
Opx
Cpx
Cpx
S
23DP10
F
S
23DP16
G
Qm
S
23DP17
H
Lvg
K
Pl
K
Qm

Figure 6. Panels A-E: Characteristic thin section images from CRO in Del Puerto Canyon. Panels F-H: characteristic thin section images from Franciscan subduction complex in Del Puerto Canyon. Magnification for samples is 4x, and the scale bar in the top left corner is 500 microns and contains the sample name. The exception is Panel D which is 20x magnification and the scale bar represents 100 microns. Images were all taken under cross polarized light (XPL). K: Potassium feldspar, Pl: plagioclase, Lvm: volcanic, microlitic, Lvl: volcanic, lathwork, Ca: calcite, Qp: polycrystalline quartz, Qm: monocrystalline quartz, Opx: orthopyroxene, Cpx; clinopyroxene, S: serpentinite.

Lu-Hf Geochemistry

Five sandstones from Del Puerto Canyon from two age groups (160-140 Ma and 100-90 Ma) were analyzed for Lu-Hf geochemistry (Figure 2, 7). These populations were chosen to reflect the general depositional age groupings of the Knoxville (latest Jurassic-earliest Cretaceous) and Panoche (earliest Late Jurassic) Formations. We analyzed a total of 96 zircons for Lu-Hf, with 53% (n = 51) of the grains crystallized from 160-140 Ma, and 47% (n = 45) from 100-90 Ma. The εHf values for the older zircons range from –17 to +16 (Figure 7), with the majority (88 %) plotting above the CHUR reference line. Within the 160-140 Ma zircons, the Knoxville Formation sample, 23DP06, has the smallest εHf range: +10 to +15 (Figure 7). Grains from the Panoche sample, 23-DPC-33, ranges from –17 to +9, with 68% of grains plotting above the CHUR reference line in older zircons (Figure 7). Older grains from the Franciscan subduction complex sample, 23DP12, range from +1 to +16, primarily overlapping with zircons of the Knoxville Formation. Late Cretaceous zircons from the Panoche Formation and Franciscan are more evolved with εHf values ranging from –13 to +15. The 100-90 Ma grains from Panoche samples are clustered around the CHUR reference line, with 90% of grains ranging from -6 to +1 (Figure 7). Zircon grains from the Franciscan subduction complex sample,

23DP12, are increasingly negative (-8 to –13) as compared to zircons from the coeval Panoche Formation.

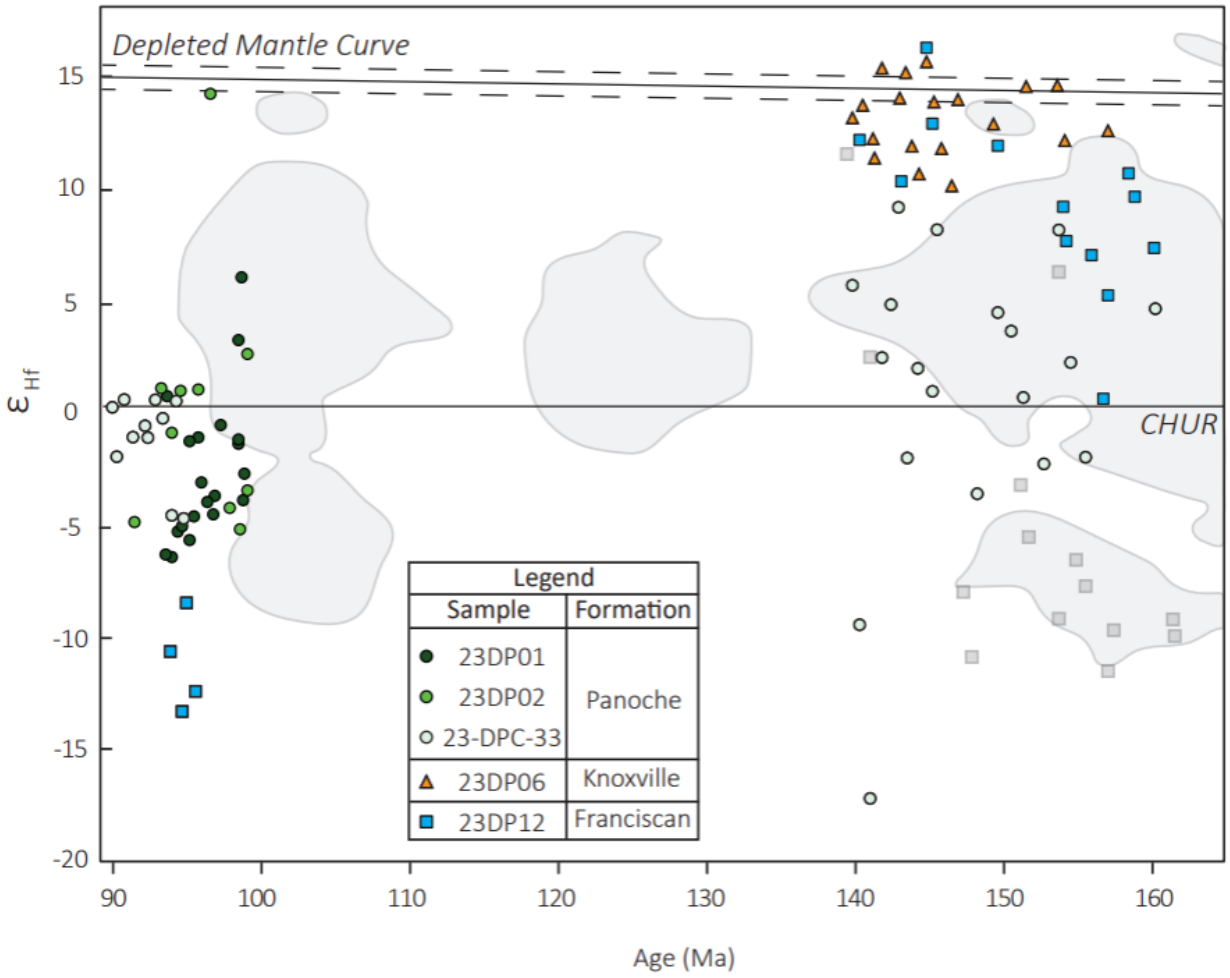

Figure 7. Epsilon Hafnium (εHf) versus U-Pb for samples from Del Puerto Canyon in age ranges of 100-90 Ma and 160-140 Ma. CHUR is chondrite uniform reservoir. Grey polygons indicate the εHf curve at 95% confidence of Sierra Nevada arc from Attia et al. (2020). Gray squares represent Western Sierra Nevada Metamorphic Belt samples from Attia et al. (2020).

Zircon Trace Element Geochemistry

The Th/U concentrations of the subset of Mesozoic zircons analyzed for Lu-Hf geochemistry were also investigated to aid with provenance interpretation (Figure 8). These

samples consist of three Panoche samples (23DP01, 23DP02, and 23-DPC-33), one Knoxville sample (23DP06), and one Franciscan subduction complex sample (23DP12). All samples, regardless of age or formation, plot within the felsic melt zone, with one outlier grain that lies within the transition zone (Figure 8). Zircons from the Panoche Formation have the widest spread of Th/U ratios, ranging from ~0.2 to 0.9, excluding an outlier with a ratio of 1.43. Zircon grains from the Knoxville Formation are densely clustered and range from ~0.1 to 0.4, and the Franciscan subduction complex sample grains range from ~0.2 to 0.7 (Figure 8). Comparing U-Pb and Th/U of all ~5,000 zircons analyzed by LA-ICP-MS indicate no change in Th/U concentrations between the pre-Mesozoic and Mesozoic grains (Appendix F); the entire dataset is not shown in Figure 8 for the purposes of clarity.

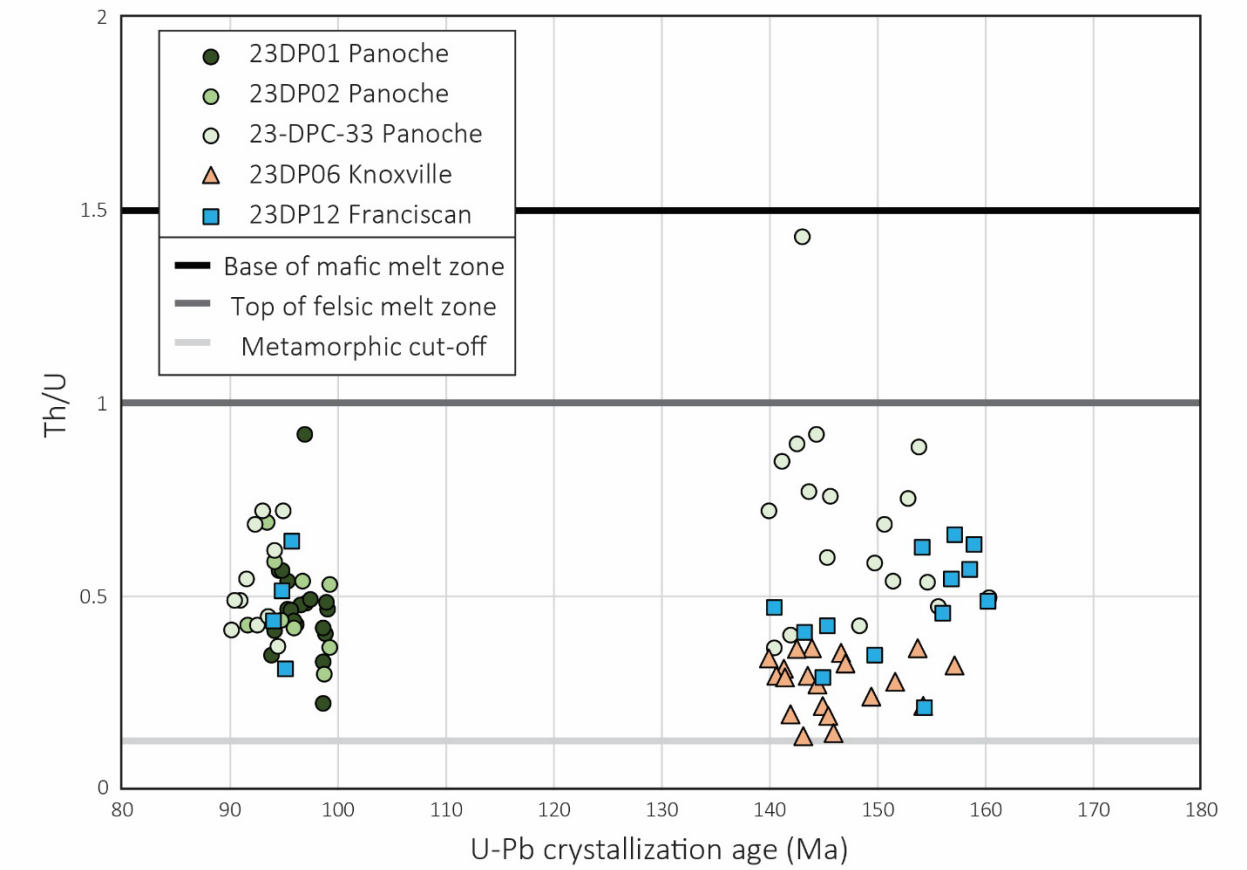

Figure 8. U-Pb crystallization age versus Th/U ratios of selected zircon grains from Del Puerto Canyon analyzed with LA-ICP-MS. The lines indicating the base and top of the mafic melt zone and the metamorphic cut off are from Teipel et al (2004) and Linnemann et al. (2011). See Appendix F for plot of all grains U-Pb versus Th/U.

Whole Rock Trace Element Geochemistry

Within REEs shown in a chondrite-normalized spider diagram, there is a negative trend and a significant negative Eu anomaly for all samples (Figure 9A). From La to Sm, the Panoche samples yield the highest concentrations with the Knoxville close below, and the CRO samples have the least concentrated values (Figure 9A).

On a La-Th-Sc ternary diagram, all samples plot between La and Sc, and far from Th (Figure 9B). There is trend with age whereby the CRO samples plots between MORB and

continental arc references, Knoxville samples right above the continental arc signature, and Panoche samples plot between UCC, and NASC reference points (Figure 9B), reflecting an increase in compositional maturity through time. Samples from the Panoche Formation are consistent with Upper Cretaceous San Joaquin Valley mudstones from Surpless (2014), but the Knoxville samples plot above the trend for Lower Cretaceous samples from the same study.

A comparison of Zr/Sc versus Th/Sc shows the CRO samples close to the andesite reference (Figure 9C). The Knoxville samples plot above andesite and the Panoche samples show a trend toward the granodiorite reference (Figure 9C). As in the La-Th-Sc ternary diagram, samples from the Panoche Formation plot with Upper Cretaceous samples from Surpless, 2014, with the Knoxville just below this trend, and the CRO samples plot with Lower Cretaceous samples from the same study.

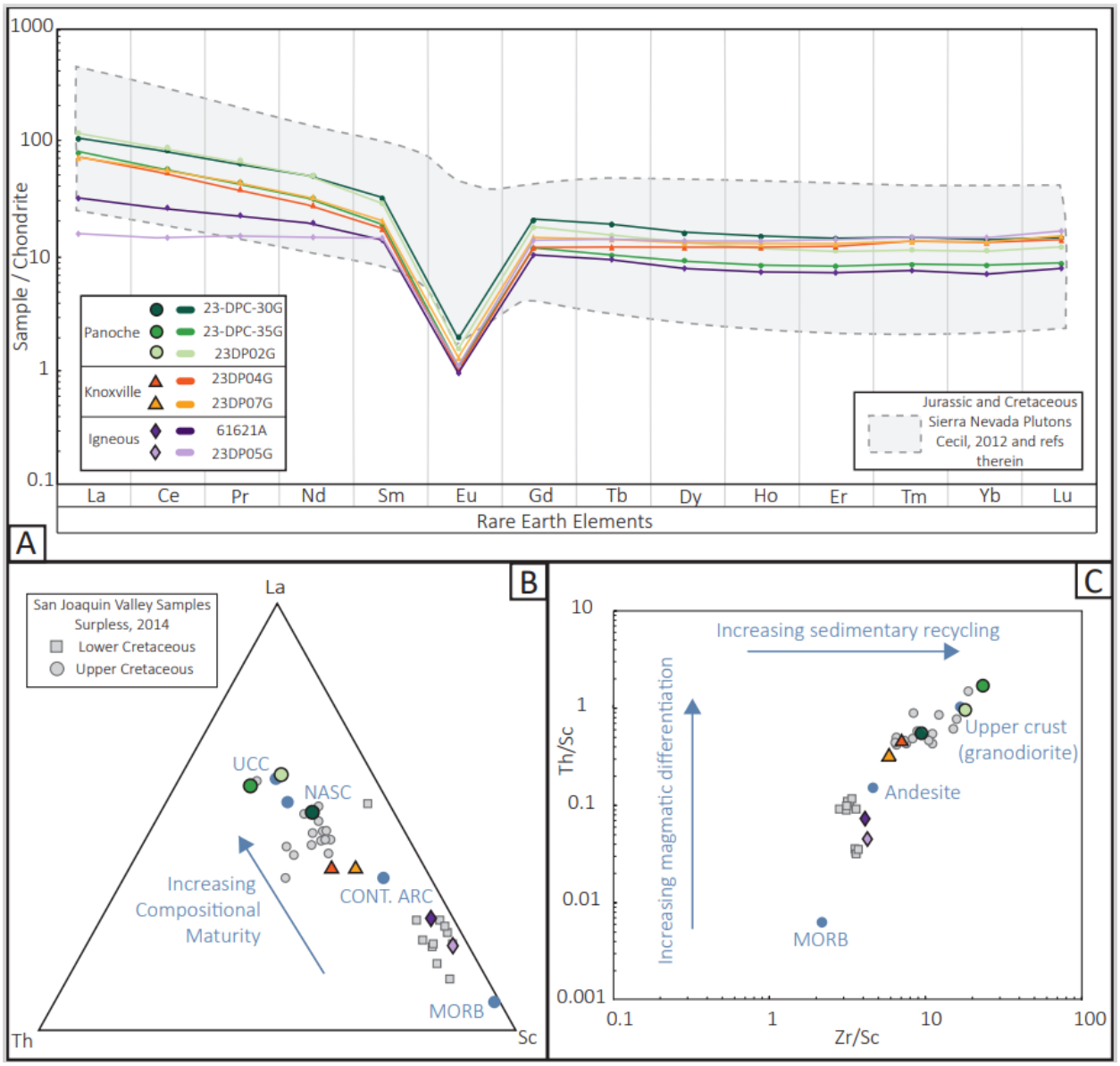

Figure 9. Geochemistry of Del Puerto GVG strata and igneous samples. (A) Spider diagram of REE (rare earth elements) normalized to chondritic reservoir (Sun and McDonough, 1989). The grey envelope with dotted border overlying the REE concentrations represents compiled Jurassic and Cretaceous aged Sierra Nevadan plutons from Cecil et al. (2012) and references wherein (B) La-Th-Sc ternary plot with potential sources from Taylor and McLennan (1985) and McLennan et al. (1993). (C) La/Sc versus Zr/Sc plot, after McLennan et al. (1990); Values for upper crust granodiorite from Taylor and McLennan (1985) and MORB from Sun and McDonough (1989). Data from Upper and Lower Cretaceous strata from Surpless (2014) shown in grey in panels B and C. The legend in Panel A is applied to all panels.

DISCUSSION

Revised Mapping

Compiling previous work by Dibblee (1982; 2007), Maddock (1964), and Raymond (1973) with our field observations and the California State Geologic map (Jennings, 1997; Wills et al. 2015), we present a revised map that incorporates previous field mapping with the results of this study in Figure 1. We find the Lotta Creek Formation does not reach the present location of Del Puerto Canyon Road and moved the contact further south to reflect this. In addition, we find GVG strata at the easternmost contact with the CRO has lithofacies, sandstone compositions, and geochronologic ages consistent with the Knoxville Formation, and re-establish the presence of this unit at this contact (see below for details). We incorporated the CRF and TOF mapped by Raymond (1973) on our map and the addition of one unnamed fault in the southeast portion of the map that was originally mapped by Dibblee (1982; 2007) (Figure 1).

Controls on Depositional Age

Sample 23DP21, collected from strata mapped as Knoxville on all previously published maps and along the western limb of the Del Puerto Keratophyre anticline, stratigraphically above the Lotta Creek Tuff, contains exclusively Mesozoic grains with MDA of 145.56 ± 1.52 Ma (Figure 1, 3, and 4). Similarly, five samples (61621B, 23DP04, 23DP03, 61621C, 23DP06) collected on the east limb of the anticline, at the contact with the CRO, yield unimodal peaks with MDAs ranging from ~139-146 Ma (Figure 1, 3, and 4). These sandstones were collected within ~ 300 m of stratigraphy comprising fissile black shales interbedded with fine-grained sandstone intervals and scattered limestone concretions. Previous mapping assigns these rocks to

the Panoche Formation (Dibblee, 1982; 2007) or an Albian Shale (Bennison et al., 1991). However, due to similarities with Knoxville sedimentary descriptions, unimodal age spectra, and ~145 Ma MDAs, we re-assign these to the Knoxville Formation (Figures 1-4). Similarly, on the western side of the Del Puerto Keratophyre anticline, along Del Puerto Canyon Road, sample 61721A was collected from similar lithofacies of shales and fine-grained sandstones interbedded with limestone boulder size concretions (Figures 2, 3). Given the similar lithofacies, the unimodal Mesozoic age distribution, and an MDA of 145.13 ± 0.11 for 61721A, we re-assign sample 61721A to the Knoxville Formation (Figure 1-4). Furthermore, we interpret these MDAs as approximating TDA and not significantly younger than ~140 Ma based on the presence of Valanginian-Hauterivian strata overlying the Knoxville Formation just south of our field area at Pacheco Pass and Coalinga.

The five sub-surface Panoche samples (23-DPC-30, 23-DPC-33, 23-DPC-34A, 23-DPC-34B, and 23-DPC-35) and two surficial Panoche samples (23DP01, 23DP02) are consistent with each other, yielding MDAs ranging from ~97-84 Ma, consistent with published depositional age. The ~40 myr duration between deposition of Lower Cretaceous Knoxville strata and Upper Cretaceous Panoche strata highlights a previously documented unconformity between strata of this age and its implications are discussed further below (Figures 3, 4). Four sandstones from Franciscan subduction complex (23DP12, 23DP11, 23DP17, and 23DP16) yield MDAs that range from ~84 to 115 Ma, which, apart from the oldest ~115 Ma MDA (23DP11), temporally overlap with deposition of the Panoche Formation. Detrital zircon age distributions from metasandstones at neighboring localities in the northern Diablo Range report MDAs between ~115-93 Ma (Dumitru et al., 2018), with Apen et al. (2021) assigning rocks with MDAs between

115-110 Ma and 100-92 Ma to the Angel Island accreted units in the Tiburon Peninsula ~100 km north of Del Puerto Canyon; restoring Cenozoic strike-slip deformation places these units ~30-50 km south of the Diablo Range (Apen et al., 2021). Two of our samples (23DP12 and 23DP17) have MDAs and DZ age spectra (discussed below) consistent with rocks of the Northern Diablo Range, whereas sample 23DP11 yields an MDA of ~ 115 Ma and age spectra consistent with metasandstones of Angel Island accreted units (Apen et al., 2021; Figure 10). Sample 23DP16 yields an MDA (~84 Ma) younger than previously reported MDAs of the Franciscan subduction complex exposed within the northern Diablo Range.

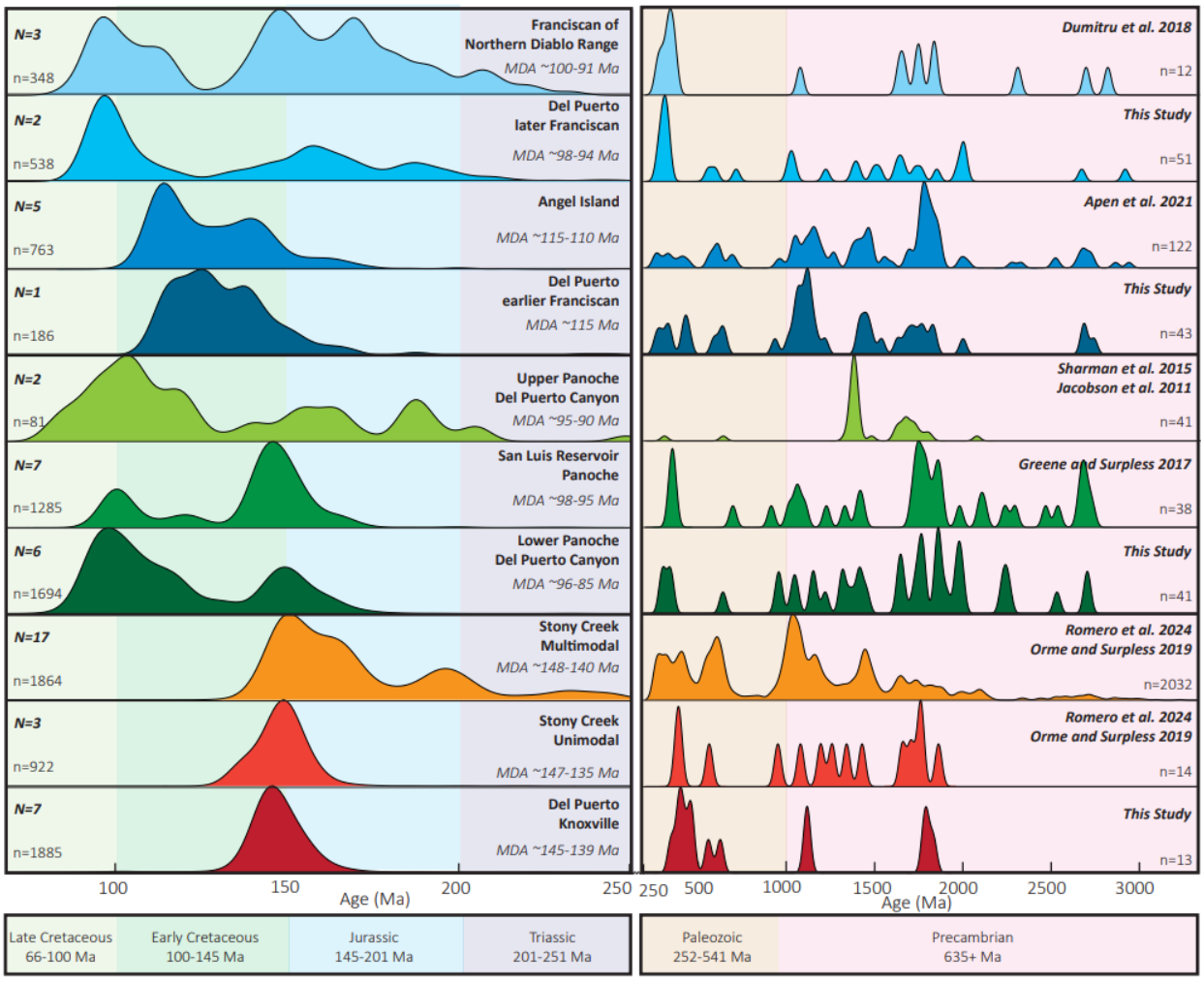

Figure 10. Detrital zircon kernel density estimates (KDEs) compilation of Franciscan subduction complex, Panoche Formation, and Knoxville Formation from the GVF. KDEs are grouped by formation, and within each formation, by age, with the oldest on the bottom of each formation. Mesozoic KDEs (50-250 Ma) are normalized to each other and have a kernel of 4. Following a break in scale, Paleozoic and Precambrian (251-3000 Ma) KDEs are normalized to each other and have a kernel of 20. References for each dataset are listed in bold italics, dataset names are listed in bold text, the MDAs for each dataset are listed in italics underneath the dataset name, samples used are represented by "N=", and total grains for each KDE are shown as "n=".

Provenance

Knoxville Formation

The Knoxville samples' unimodal DZ U-Pb age spectra (Figure 3) and relative reduction in volcanic lithics as compared to the majority of the oldest GVG in both the Sacramento and SJV basins (Figure 5) suggests that there was a plutonic point source of broadly uniform age during deposition, potentially a Jurassic pluton ~146-139 Ma within the central or southern Sierra Nevada magmatic arc, including potential Jurassic sources within the Western Sierra Nevada Metamorphic Belt (WSNMB) (Ingersoll, 2000; Cecil et al. 2012; Schweickert, 2015) or the underlying CRO (e.g. Ingersoll, 1982; Romero et al., 2024). A unimodal Mesozoic age peak contrasts with much of the oldest, most-basal GVG in the northern GVF, the Stony Creek Formation, which commonly shows >55% pre-Mesozoic grains (Figure 10; Orme and Surpless, 2019: Romero et al., 2024). Nevertheless, few samples from the Stony Creek Formation within the Sacramento basin also show a similar unimodal peak at ~145-150 Ma and no pre-Mesozoic grains (DeGraaff-Surpless, 2002; Surpless et al. 2006; Orme and Surpless, 2019); these samples are also interpreted to reflect contributions from a point-source within the proximal undissected magmatic arc (Ingersoll, 1982; DeGraaff-Surpless, 2002; Romero et al., 2024).

Four of our Knoxville Formation samples contain pre-Mesozoic grains found within basement terranes of North America and are petrographically similar to the basal GVG samples from the Sacramento basin that contain abundant pre-Mesozoic detrital zircon grains (Dickinson and Rich, 1972; Ingersoll, 1983; Surpless, 2014; Romero et al. 2024). We interpret that deposition of the oldest GVG strata in the San Joaquin basin, the Knoxville Formation, occurred proximal to North America, which is consistent with previous studies that of the oldest GVG in the Sacramento basin (DeGraaff-Surpless, 2002; Orme and Surpless, 2019). In addition, the presence of 161 total detrital olivine grains found in all five of our Knoxville sandstone petrographic analyses suggests that the CRO may have provided an additional source of detritus, as suggested by Romero et al. (2024) for the most basal Stony Creek Formation overlying the CRO in the Sacramento basin.

Our zircon and whole rock geochemical results support linking the Knoxville Formation to the Sierra Nevada continental arc during Knoxville deposition, consistent with geochemistry of coeval GVG strata Surpless (2014) and records from the Sierra Nevada magmatic arc and the western Sierra Nevada magmatic belt (Attia et al., 2020; 2021) (Figure 8 and 9). This is most apparent by La-Th-Sc and Zr/Sc versus Th/Sc plots, in which Knoxville samples plot between continental arc and upper continental crust signatures (McLennan, 1985; McLennan et al., 1993), and in between andesite and upper crust signatures (Taylor and McLennan, 1985). Rare Earth Element spectra of central and southern Jurassic Sierra Nevada plutons display concave to flat trends with large some outliers showing a negative Eu anomalies due to high SiO2 intrusions (Cecil et al., 2012 and references therein), which aligns with the Jurassic strata from the Knoxville Formation in Del Puerto Canyon (Figure 9A). Interestingly, the zircon εHf values

from Knoxville zircon overlap with data points from the Sierran arc but show a shift to slightly more juvenile values as compared to the 95% confidence interval from the arc (Figure 7; Attia et al., 2020). These values are more consistent with a more juvenile source such as the CRO and accreted island-arc material of the WSNMB, but as we only analyzed one sample from the Knoxville for Lu-Hf and whole-rock and zircon U-Pb geochemical data support a link with a felsic continental arc, we interpret the CRO and WSNMB as secondary sources to Jurassic plutons of the Sierra Nevada.

Panoche Formation

We interpret no major provenance changed during Panoche deposition (Figure 3, 4), based on three lines of evidence: the Panoche MDAs generally young up section (west to east) or remain the same, the Panoche age spectra are similar to each other, with Middle-Late Jurassic (~170-145 Ma) and Early-Late Cretaceous (~140-90 Ma) prominent age populations (Figure 3), and the Panoche sandstone samples have similar petrologic compositions (Figure 5). The abundant Cretaceous zircons coincide with the well-documented mid-Cretaceous high flux magmatism of the Sierra Nevada, which comprise ~50% of all exposed plutons within the Sierran arc today (e.g., Chen and Moore, 1982; Ducea et al., 2015; Paterson and Ducea, 2015). These include proximal plutons of the Tuolumne Intrusive Suite, adjacent to the dextral Bench Canyon and Quartz Mountain shear zones, both of which are interpreted to be active during Campanian Panoche Deposition (e.g., Coleman et al., 1994; McNulty, 1995; Tobisch et al., 1995; Tikoff and Greene, 1997; Greene and Surpless, 2017; Tomek et al., 2024). By contrast, Jurassic sources are less abundant and spatially scattered within the modern outcrop of the Sierra Nevada. The presence of the same late Jurassic age peak (~150 Ma) and similarities between the

petrography of both Knoxville and Panoche Formations suggests that during Panoche deposition, Jurassic sources that fed the Knoxville were still feeding the GVF (e.g., Dumitru et al., 2015; Green and Surpless, 2017). The age range of Jurassic grains (~170-146 Ma) present in our samples is found within the Jurassic Sierra Nevada arc and WSNMB, and is also are abundant in various parts of the CRO, including at Del Puerto Canyon where crystallization ages range from ~161-155 Ma (Lanphere, 1971; Hopson et al., 1981; Evarts, 1992; Mattinson et al., 2008).

Our samples are down-section, either in outcrop or in the sub-surface, and yield MDAs older than two sandstones from the Panoche Formation analyzed by Sharman et al. (2015) and Jacobson et al. (2011), which are Campanian in age (Figure 10). These samples yield similar Mesozoic age peaks, but outcrop sample GVG09-2 from Sharman et al. (2015), contains Proterozoic grains between ~1330-1400 Ma and ~1600-1800 Ma. These peaks, notably grains circa 1380 Ma are interpreted to be derived from pluton within the Lemhi subbasin of Idaho and were transported to the GVF basin and Franciscan subduction complex between ~85-80 Ma via the Kione River (Dumitru et al., 2016). Given the lack of the ~1380 Ma peak in our samples, and their lower stratigraphic position, we propose the lower Panoche Formation did not receive detritus from the Kione River system until its arrival after 85 Ma.

At Del Puerto Canyon, Bishop (1970) interpret conglomerate clast counts as indicating a potential western source for detritus, such as the bathymetric high of the Franciscan subduction complex. We could not directly test this with additional geochronologic and geochemical data due to lack of access to the conglomeratic ridges in our field area. However, other locales in the San Joaquin Valley, including the exposures of the Panoche Formation at San Luis Reservoir ~45 km southwest of Del Puerto Canyon, indicate a predominantly west or southeast-directed

current (Ingersoll, 1979; Cherven, 1983: Bennison, 1991; Bennison et al., 1991; Greene and Surpless, 2017). At San Luis Reservoir, Greene and Surpless (2017) document both felsic and mafic plutonic rocks (granitoids to gabbro) and metavolcanic and/or metavolcaniclastic rocks, and interpret the latter as derived from the CRO and/or the WSNMB. Our petrographic results from the Panoche Formation overlap with those of Greene and Surpless (2017) and other the SJV Grabast petrofacies of Mansfield (1979) and Ingersoll (1983) and include similar diagenetic features such as presence of calcite cement, altered volcanic grains, and dissolved feldspar grain boundaries. However, we do not observe a high abundance of metamorphic grains as are observed by Ingersoll (1983). The abundance of potassium feldspar to total feldspar in all of our samples are consistently 50%, unlike the 0 to 50% increase from Jurassic to Cretaceous found by Ingersoll (1983). Panoche samples are geochemically more compositionally mature and more evolved than Knoxville samples (Figure 9), but both formations' geochemical signals tie their provenance to the Sierra Nevadan arc, as seen in the overlap of Del Puerto GVG strata eHf with the Sierran arc signature (Figure 7; Attia at al., 2020), felsic zircon Th/U ratios (Figure 8), and the REE trends of central and southern Cretaceous Sierra Nevada plutons (Figure 9; Cecil et al. 2012). Integrating the petrographic, geochronologic, and geochemical data with the paleocurrent data from previous studies, we favor proximal Sierra Nevada Cretaceous and Jurassic plutons as the primary source of sediment for the Panoche samples at Del Puerto Canyon. However, we do not dismiss the WSNMB as another potential source, especially given its spatial relationship to the plutons of the Sierra Nevada and similar εHf range as WSNMB.

Franciscan Subduction Complex

Franciscan subduction complex sandstones share similar framework grains with the Panoche Formation in Del Puerto Canyon (Figures 5, 6), but also contain accessory detrital serpentinite (Figure 6), which is not observed in our Panoche sandstones. The MDAs of the Franciscan subduction complex sandstone coincide with the Panoche MDAs (Figure 4), but age spectra contain more pre-Mesozoic grains (~6-52%) than the Panoche or Knoxville samples (Figure 3). These data are consistent with previous studies on the Franciscan subduction complex that show an abundance of syn-volcanic and pre-Mesozoic age grains (Apen et al., 2021; Dumitru et al., 2015; Snow et al., 2010) that are interpreted to represent clastic sedimentation from the North American margin (e.g., Dumitru et al., 2018; Wakabayashi, 2015). Pre-Mesozoic grains (~250-450 Ma, ~1000-1200 Ma, ~1400-1600, ~1600-1800, and a few >2000 Ma grains) are found in samples with MDAs between ~115-94 Ma. These age populations are consistent with original derivation from the Appalachian orogen, Grenville Province, anorogenic granitic plutons, Yavapai-Mazatzal Provenance and older Paleoproterozoic North American basement (e.g., Dickinson et al. 2012; Gehrels and Pecha, 2014). Notably, 23DP16, differs in having two major Proterozoic age populations between ~1330-1470 Ma and ~1600-1800 Ma, which is consistent the Campanian Panoche sample of Sharman et al. (2015) (Figure 10). Following the pioneering observations of Dumitru et al. (2016), we interpret 23DP16 to also record the arrival of the Kione River system, sourced from central Idaho to the Franciscan subduction complex after 85 Ma.

Detrital zircon age distributions from neighboring localities of the Franciscan in the northern Diablo Range have MDAs between ~104-93 Ma, with prominent age peaks at ~160-140 Ma and ~120-115 Ma (Dumitru et al., 2018) and abundant pre-Mesozoic grains that lack the

~1380 Ma Kione signal. Our three Franciscan samples with MDAs between ~115-94 Ma have age spectra consistent with these prior samples and support correlations with the Angel Island or Alcaraz accreted terranes. Interestingly, εHf data on one sample (23DP12) from the Franciscan subduction complex show overlap of Jurassic age grains with GVG strata and the Sierran arc signature but show more evolved signatures for four Cretaceous grains relative to the GVG (Figure 7; Attia et al., 2020). This general pull-down in εHf space, although only evident from four grains, is consistent with the Hf isotopic signatures of North American basement (e.g., Gehrels and Pecha, 2014), and does not require input from the Kione Rive system sourced in the Idaho region, which we interpret to arrive after deposition of these samples and at the time of deposition of sample 23DP16, ~ 84 Ma.

Tectonic Implications

In Del Puerto Canyon, the crystallization age of the CRO is ~161-149 Ma (Lanphere, 1971; Hopson et al., 1981; Evarts, 1992; Mattinson et al., 2008), which is generally consistent with other CRO ophiolite fragments (see summary in Arkula et al., 2022). The uppermost CRO and overlying Lotta Creek Tuff are dated to ~149 Ma (Evarts, 1992), indicating a ~ 2-5 myr unconformity between the CRO/Tuff Knoxville Formation (149-145.56 ± 1.42). The presence of accessory olivine in the Knoxville Formation in Del Puerto Canyon indicates that the CRO was exposed as a source of sediment during the initiation of forearc deposition. Similar petrographic and age relationships are observed in the northern GVF at Crowfoot Point, where the most basal GVG, the Stony Creek Formation, is petrographically indistinguishable from an underlying breccia interval that was derived from the CRO west of Paskenta in the Sacramento Basin (Romero et al., 2024).

The geochemical signatures of the Del Puerto Canyon CRO samples (61621A and 23DP05G) plot between MORB and continental arc on a Th-La-Sc ternary diagram, and closer to andesite than MORB on a Zr/Sc versus Th/Sc plot (Figure 9). In addition, the CRO samples generally follow the same REE trends as Jurassic and Cretaceous plutons from northern, central, and southern Sierra Nevada (Figure 9A; Cecil et al., 2012), apart from the flat light REE spectra for 23DP05G. Our petrographic and geochemical results are consistent with previous studies on the CRO at Del Puerto Canyon, are inconsistent with formation at a mid-oceanic ridge setting, and suggest an island-arc or suprasubduction zone are more likely candidates for the origin of the CRO as seen by the silicic and plutonic components of the CRO at Del Puerto Canyon (Evarts, 1977; 1978; Dickinson et al., 1996; Evarts et al., 1999). Notably, the CRO samples from Del Puerto Canyon plot amongst Lower Cretaceous strata from further south within the SJV (Surpless, 2014; Figure 9C). Surpless (2014) proposed the southwestern Sierra Nevada foothills as a potential source for more MORB-like materials due to the abundance of metavolcanics and zircon poor (i.e., more mafic) sources. We note that overlap between our CRO samples and the Lower Cretaceous strata of Surpless (2014) broadly supports our interpretation that the basal GVG in the SJV basin received input from the CRO, in addition to metavolcanic sources within the WSNMB and plutons of the Sierran magmatic arc. However, our Knoxville samples plot closer to the continental arc and within the lower part of the upper granodiorite crust of these discrimination plots. One explanation for this difference may be that Del Puerto is located farther north than the Lower Cretaceous SJV strata studied by Surpless (2014), and that the proposed southern sources did not reach this far north.

The Knoxville Formation records the earliest GVG sedimentation atop the CRO, ~2-5 myr after the CRO crystallized, and was sourced from the proximal Sierra Nevada magmatic arc and western foothills, within minor input from the CRO as seen by the abundance of detrital olivine (Figure 5F, 11A). The presence of detrital olivine in our Knoxville samples indicates that the CRO is exposed and had not undergone hydrothermal alteration to serpentinite (Rai and Matthew, 2021) The Knoxville Formation appears to be more extensively preserved at Del Puerto Canyon than in other regions of the SJV, yet is significantly thinner than the latest Jurassic-earliest Cretaceous Stony Creek Formation, which forms the basal strata of the GVG in the northern GVF (Moxon, 1988). Given the lack of evidence for significant accretionary processes at the Franciscan trench during Knoxville deposition (Dumitru et al., 2010; Mulchay et. al., 2018), the SJV part of the GVF may have been a sloped forearc with a minor trench slope break to trap sediment behind it (Dickinson and Seely, 1979; Dickinson, 1995; Figure 11). After the proximal sedimentation of the Knoxville Formation, the sloped forearc may have transitioned from underfilled to filled, leaving no room for more sediments to accumulate, and causing sediment to bypass to the trench or nearby basins in the GVF (Figure 11B).

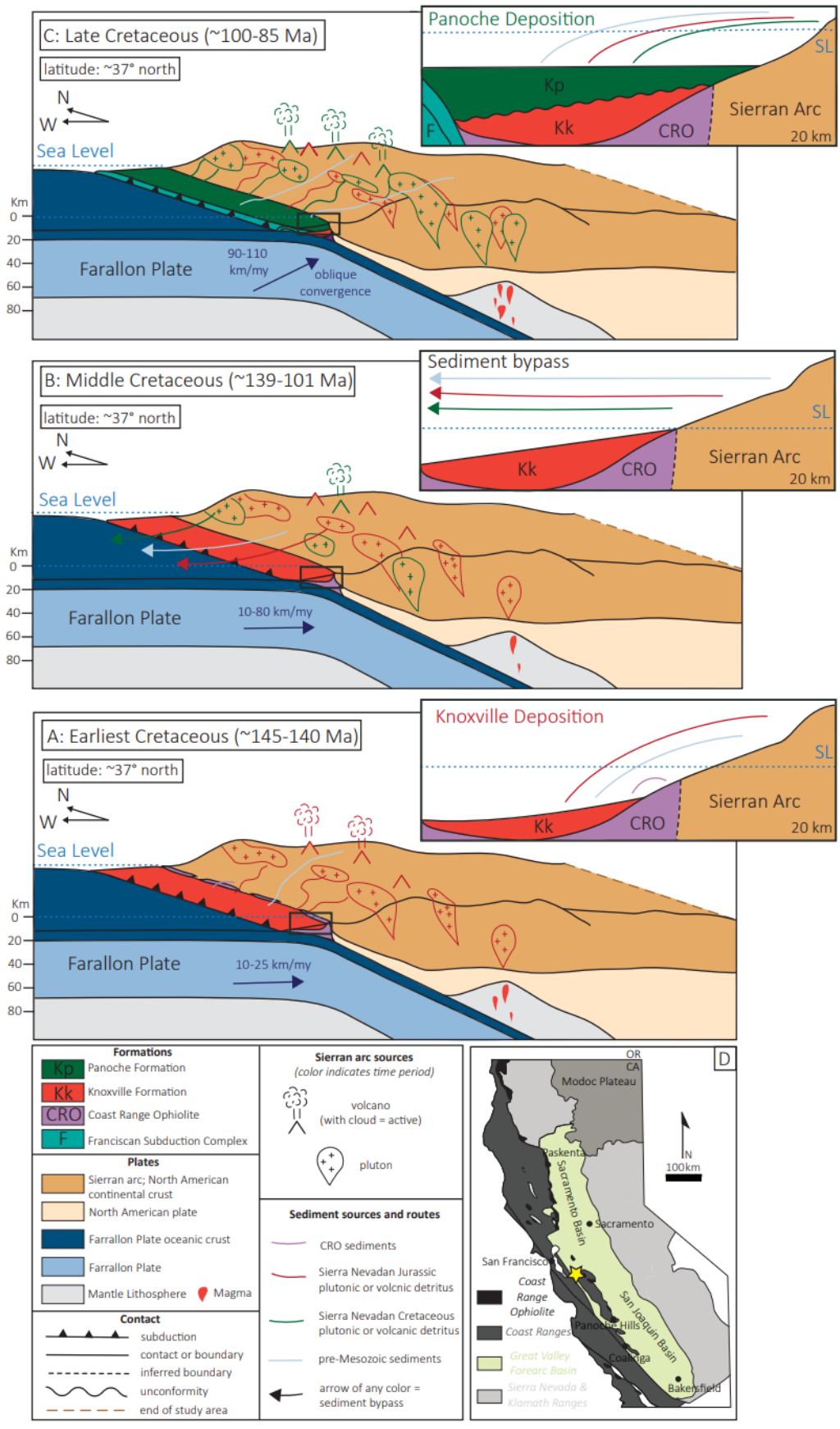
C: Late Cretaceous (~100-85 Ma)
latitude: ~37° north
N
W
Sea Level
Km
0
20
40
60
80
Farallon Plate
90-110 km/my
oblique convergence
Panoche Deposition
SL
Kp
Kk
CRO
F
Sierran Arc
20 km
B: Middle Cretaceous (~139-101 Ma)
latitude: ~37° north
Sediment bypass
10-80 km/my
A: Earliest Cretaceous (~145-140 Ma)
latitude: ~37° north
Knoxville Deposition
10-25 km/my
Formations
Kp Panoche Formation
Kk Knoxville Formation
CRO Coast Range Ophiolite
F Franciscan Subduction Complex
Plates
Sierran arc; North American continental crust
North American plate
Farrallon Plate oceanic crust
Farrallon Plate
Mantle Lithosphere
Magma
Contact
subduction
contact or boundary
inferred boundary
unconformity
end of study area
Sierran arc sources
(color indicates time period)
volcano (with cloud = active)
pluton
Sediment sources and routes
CRO sediments
Sierra Nevadan Jurassic plutonic or volcnic detritus
Sierra Nevadan Cretaceous plutonic or volcanic detritus
pre-Mesozoic sediments
arrow of any color = sediment bypass
D
OR
CA
Modoc Plateau
Paskenta
Sacramento Basin
Sacramento
N
100km
San Francisco
Coast Range Ophiolite
Coast Ranges
Great Valley Forearc Basin
Sierra Nevada & Klamath Ranges
Panoche Hills
San Joaquin Basin
Coalinga
Bakersfield

Figure 11. Tectonic model of the GVF at Del Puerto Canyon (latitude of ~37° north) in the San Joaquin Basin during (A) earliest Cretaceous, (B) middle Cretaceous, and (C) Late Cretaceous. Lithospheric scale 3-D overview and a zoomed in cross section of the forearc depositional center shown for each time interval. Legend applies to all panels and insets. Panel D is a generalized geologic map of California, and the yellow star indicates the general latitude of the tectonic models. Convergence rate (normal component) and angle of obliquity from Engebretson, Cox, Gordon (1985).

The end of the ~40 Ma unconformity from ~140-100 Ma recorded in GVG strata of Del Puerto Canyon (Figures 3, 11B) coincides with a regionally documented unconformity at ~105-100 Ma (DeCelles and Graham, 2015; Moxon, 1988), but includes the interval of deposition of the Platina and Lodoga Formations in the Sacramento Valley (~132-100 Ma) (e.g., Ingersoll, 1979; Ingersoll, 1983). In addition, Lower Cretaceous (Valanginian-Hauterivian) strata are preserved in the Coalinga area of the SJV, ~170 km south of Del Puerto Canyon (Moxon, 1988). The Del Puerto Canyon unconformity spans an interval of reduced magmatism within the Sierra Nevada, non-accretion at the trench at the latitude of the SJV, and little to no high T metamorphism (e.g., Patterson and Ducea, 2015; Dumitru et al., 2018; Mulchay et al., 2018; Apen et al., 2021). A potential interpretation of this long unconformity is that erosion rates were low during the magmatic-lull and there was no mechanism to capture sediment between the latitude of Mt. Diablo and the Panoche Hills part of the SJV during ~90-140 Ma, leading to a period of sediment bypass (Figure 11B). This is consistent with the Early Cretaceous depocenter in the GVF in Sacramento basin, where Lower Cretaceous sediments accumulated, at low sediment flux (e.g., Moxon, 1988; Orme and Graham, 2018). Notably, during this same period, the Franciscan records accretion of the South Fork Mountain Schist and Yolla Bolly terranes outboard of the northern GVF (e.g., Worrall, 1981; Dumitru et al., 2018). In addition, successions of Upper Cretaceous rocks are thickest in the San Joaquin basin compared to the

Sacramento basin. This spatial shift in deposition is observed in both subsurface and in outcrop studies and supported by observed southward down-lap geometries (Moxon, 1988; Orme and Graham, 2018). This interpretation suggests the forearc may have been segmented into isolated depositional centers, as is common in the recent ancient to modern forearc records along the Java-Sumatra, Aleutian, and Japanese island arc systems (e.g., Schlüter et al. 2002; Yang and Gao, 2020; Okamura and Shishikura, 2020; Utsunomiya et al., 2023).

An alternative hypothesis to explain the development of the unconformity is that sediments of Lower Cretaceous age were deposited in the San Joaquin Valley, but subsequently eroded. Greene and Surpless (2017) discuss evidence from Tagami and Dumitru (1996) for rapid exhumation of the Franciscan wedge near Mt. Hamilton, ~30 km west of our study area, during ~100-70 Ma, as a potential mechanism to erode Lower Cretaceous strata. Importantly, this model is invoked to explain the CRO as a potential source of the Panoche Formation based on the abundance of metavolcanics within clast counts at San Luis Reservoir (Greene and Surpless, 2017). Our sandstone petrographic work does not support the CRO as a source for the lower Panoche Formation, and instead, we propose slight provenance differences between the lower pre-Campanian Panoche at Del Puerto Canyon and Campanian Panoche Formation up-section at Del Puerto Canyon (Sharman et al. 2015) and at San Luis Reservoir (Greene and Surpless, 2017). Application of low-temperature thermochronology strata preserved across the Lower-Upper Cretaceous contact could shed light on any record of basin uplift and erosion not present in the preserved stratigraphic record.

Deposition of the Panoche Formation occurs at a time of 1) increased plate convergence and obliquity (e.g., Engbretson, Cox, and Gordon, 1985), 2) flare-up in arc magmatism, and 3)

wedge accretion and exhumation of high-grade blocks within the wedge (e. g., Patterson and Ducea, 2015). The latter is consistent with the Franciscan complex preserved in Del Puerto Canyon and elsewhere in the Diablo Range (e.g., Apen et al. 2021; Dumitru et al. 2018). Once the Franciscan subduction complex transitioned to highly accretionary at ~123 Ma (Dumitru et al. 2018), it establishes an outer forearc high, or ridged forearc (Dickinson, 1995) behind which sediment shed from the Sierran arcs accumulated with the GVF basin (Figure 11C). Rapid subsidence and sediment accumulation is found during the Cenomanian across the Great Valley forearc (e.g., Ingersoll, 1978; 1982) and Moxon (1988) first correlates this to an increase in the rate of convergence and obliquity between the Farallon and North American plates (Page and Engebretson, 1984). Similarly, changes in plate obliquity have been called upon to explain Cretaceous high-flux magmatism and associated changes in igneous fabrics (e.g., Tomek et al., 2024). After ~ 85 Ma, the Panoche Formation and Franciscan subduction complex begin to receive input from the Kione River system that is sourced from the continental interior in Idaho (Dumitru et al., 2016).

CONCLUSIONS

The Late Jurassic through early Late Cretaceous geologic history of Del Puerto Canyon in central California highlights the integrated history of the Franciscan subduction complex, CRO, GVG, and Sierra Nevada magmatic arc. The most basal GVG strata in Del Puerto Canyon, the Knoxville Formation, were deposited from ~145-139 Ma, ~2-5 myr after emplacement of the CRO as its underlying basement. The Knoxville Formation was derived from the proximal felsic to intermediate plutons and Sierra Nevada magmatic arc, with minor components of mafic minerals sourced from exposed CRO. The basin was likely a sloped forearc, with little accretionary prism outboard, and may have become an overfilled basin and locus of sediment bypass shortly after deposition of the Knoxville Formation atop the CRO, resulting in a ~40 Myr unconformity with the Late Cretaceous Panoche Formation. We favor a model of sediment bypass to explain the unconformity because the time interval (~140-100 Ma) coincides with no evidence for accretionary or metamorphism within the Franciscan trench outboard of the SJV basin and during a magmatic lull in the Sierra Nevada arc, which presumably mean erosion rates were lower. At Del Puerto Canyon, the Late Cretaceous Panoche Formation and Franciscan subduction complex record a return to sedimentation and rapid subsidence and accretion along the trench, respectively. The increase in rapid sediment accumulation within the GVF basin during this time, likely reflects the growth of the accretionary prism acting as an outer forearc high behind which to trap sediments, preventing their escape into the trench. In turn, these processes are consistent with and reflect the return to high flux magmatism within the Sierra Nevada, owing to increased rates of oblique convergence (Engebretson, Cox, Gordon, 1985). After ~85 Ma, the multimodal age spectra of the Panoche

Formation, including a ~ 1380 Ma peak, indicates sediment sources from the interior of North America (i.e., Kione River from Idaho; Dumitru et al., 2016), in addition to the Jurassic sources present during initial deposition of the Knoxville Formation within the GVF basin. This study highlights the utility of integrating multiple types of datasets across different lithotectonic units preserved within an ancient forearc to better understand processes active during forearc basin initiation and rapid basin subsidence.

REFERENCES CITED

Anderson, R. V., Pack, R. W., 1915, Geology and Oil Resources of the West Border of the San Joaquin Valley North of Coalinga, California: U.S. Geological Survey Bulletin, vol. 603, 220 p.

Apen, F. E., Wakabayashi, J., Day, H. W., Roeske, S. M., Souders, A. K., Dumitru, T. A., 2021. Regional-scale correlations of accreted units in the Franciscan Complex, California, USA: A record of long-lived, episodic subduction accretion, Plate Tectonics, Ophiolites, and Societal Significance of Geology: A Celebration of the Career of Eldridge Moores, John Wakabayashi, Yildirim Dilek

Arkula, C., Lom, N., Wakabayashi, J., Rea-Downing, G., Qayyum, A., Dekkers, M.J., Lippert, P.C., van Hinsbergen, D.J., 2023. The forearc ophiolites of California formed during trench-parallel spreading: Kinematic reconstruction of the western USA Cordillera since the Jurassic. *Earth-Science Reviews*.

Armstrong-Altrin, J.S., & Verma, S.P., 2005. Critical evaluation of six tectonic setting discrimination diagrams using geochemical data of Neogene sediments from known tectonic settings. *Sedimentary Geology, 177*, 115-129.

Attia, S., Cottle, J.M., and Paterson, S.R., 2020, The erupted zircon record of continental crust formation during mantle driven arc flare-ups: Geology, v. 48, no. 5, p. 446–451, https://doi .org/10.1130/G46991.1

Attia, S., Paterson, S. R., Saleeby, J., Cao, W., 2021, Detrital zircon provenance and depositional links of Mesozoic Sierra Nevada intra-arc strata. *Geosphere,* 17 (5): 1422–1453. doi: https://doi.org/10.1130/GES02296.1

Bailey, E. H., Blake, M. C., Jr., and Jones, D. L., 1970, On-land Mesozoic ocean crust in California Coast Ranges: U.S. Geological Survey Professional Paper 700-C, p. C70–C81.

Bailey, E. H., Jones, D. L., 1964, Franciscan and related rocks, and their significance in the geology of western California: California Division of Mines and Geology Bulletin 183, 177 p.

Bennison, A.P., 1991, Great Valley Sequence east of Pacheco Pass in central California: *Geological Society of America Abstracts with Programs*, v. 23, no. 2, p. 6.

Berger, W. H., and Winterer, E. L., 1974, Plate stratigraphy and the fluctuating carbonate line, in Hsü, K. J., and Jenkyns, H. C., eds., Pelagic sediments: International Association of Sedimentologists Special Publication No. 1, p. 11–48.

Bhatia, M.R., and Crook, K.A.W., 1986, Trace element characteristics of graywackes and tectonic setting discrimination of sedimentary basins: *Contributions to Mineralogy and Petrology*, v. 92, p. 181–193, doi:10.1007/BF00375292.

Bishop, C. C., 1970, Upper Cretaceous stratigraphy of the west side of the northern San Joaquin Valley, Stanislaus and San Joaquin Counties, California: California Div. Mines and Geology Spec. Rept. 104, 29 p

Bonnardot, M.A., Hassani, R., Tric, E., Ruellan, E., and Rénier, M., 2008, Effect of margin curvature on plate deformation in a 3-D numerical model of subduction zones: Geophysical Journal International, v. 173, no. 3, p. 1084–1094, doi:10.1111/j.1365-246X.2008.03752.x.

Byrne, D.E., Wang, W.H., and Davis, D.M., 1993, Mechanical role of backstops in the growth of forearcs: Tectonics, v. 12, no. 1, p. 123–144, doi:10 .1029/92TC00618.

Cawood, P.A., Hawkesworth, C.J., Dhuime, B., 2012. Detrital zircon record and tectonic setting. Geology 40, 875e878.

Crittenden, M. D., Jr., 1951. Geology of the San Jose-Mount Hamilton area, California: California Division of Mines Bulletin 157, 74 pp.

Cecil, M.R., Rotberg, G.L., Ducea, M.N., Saleeby, J.B., and Gehrels, G.E., 2012, Magmatic growth and batholithic root development in the northern Sierra Nevada, California: *Geosphere*, v. 8, p. 592–606, doi:10.1130/GES00729.1.

Chen, J.H., and Moore, J.G., 1982, Uranium-lead isotopic ages from the Sierra Nevada batholith, California: *Journal of Geophysical Research*, v. 87, p. 4761–4784, doi:10.1029/JB087iB06p04761.

Cherven, V.B., 1983, A delta-slope-submarine fan model for Maestrichtian part of Great Valley sequence, Sacramento and San Joaquin basins, California: *American Association of Petroleum Geologists Bulletin*, v. 67, p. 772–816.

Coutts, D.S., Mathews, W.A., and Hubbard, S.M., 2019, Assessment of widely used methods to derive depositional ages from detrital zircon populations: Geoscience Frontiers, v. 10, p. 1421–1435, https://doi.org/10.1016/j.gsf .2018.11.002

Cowan, D. S., and Bruhn, R. L., 1992, Late Jurassic to early Late Cretaceous geology of the U.S. Cordillera, in Burchfiel, B., Lipman, P.W., and Zoback, M.L., eds. The geology of North America: The cordilleran orogen: Conterminous US Boulder, Colorado: The Geological Society of America, p. 169-198.

Cox, R., Lowe, D.R., and Culler, R.L., 1995, The influence of sediment recycling and basement composition on evolution of mudrock chemistry in the southwestern United States: Geochimica Et Cosmochimica Acta, v. 59, p. 2919–2940. doi:10.1016/0016-7037(95)00185-9

Crowley, J.L., Schoene, B., Bowring, S.A., 2007, U-Pb dating of zircon in the Bishop Tuff at the millennial scale: Geology 35: 1123-1126.

Clift, P.D., and Vannucchi, P., 2004, Controls on tectonic accretion versus erosion in subduction zones: Implications for the origin and recycling of the continental crust: Reviews of Geophysics, v. 42, RG2001, doi:10 .1029/2003RG000127.

Coleman, D.S., Gray, W., and Glazner, A.F., 2004, Rethinking the emplacement and evolution of zoned plutons: Geochronologic evidence for incremental assembly of the Tuolumne Intrusive Suite, California: Geology, v. 32, p. 433–436, doi:10.1130/G20220.1.

Contardo, X.J., Kukowski, N., and Cembrano, J.M., 2011, Material transfer and its influence on the formation of slope basins along the south central Chilean convergent margin: Insights from scaled sandbox experiments: Tectonophysics, v. 513, p. 20–36, doi:10 .1016/j.tecto .2011.09.016.

DeCelles, P. G., & Graham, S. A. (2015). Cyclical processes in the North American Cordilleran orogenic system. Geology, 43(6), 499–502. https://doi.org/10.1130/G36482.1

DeGraaff-Surpless, K., Graham, S. A., Wooden, J. L., and McWilliams, M. O., 2002, Detrital zircon provenance analysis of the Great Valley Group, California: evolution of an arc-forearc system. Geological Society of America Bulletin, v. 114, pp. 1564–1580.

Dickinson, W. R., and Rich, E. I., 1972, Petrologic intervals and petrofacies in the Great Valley sequence, Sacramento Valley, California. Geological Society of America Bulletin, v. 83, pp. 3007–3024.

Dickinson, W.R., 1973, Widths of modern arc-trench gaps proportional to past duration of igneous activity in associated magmatic arcs: Journal of Geophysical Research, v. 78, no. 17, p. 3376–3389, doi:10 .1029 /JB078i017p03376.

Dickinson, W.R., 1974, Plate tectonics and sedimentation, in Dickinson, W.R., ed., Tectonics and Sedimentation: Society of Economic Paleontologists and Mineralogists (SEPM) Special Publication 22, p. 1–27, doi:10 .2110/pec.74.22.0001.

Dickinson, W.R., and Seely, D.R., 1979, Structure and stratigraphy of forearc regions: The American Association of Petroleum Geologists Bulletin, v. 63, p. 2–31.

Dickinson, W. R., 1981, Plate tectonics and the continental margin of California, in Ernst, W. G. ed., The geotectonic development of California, Englewood Cliffs, Prentice-Hall, pp. 1–28.

Dickinson, W. R., 1981, Plate tectonic evolution of the southern Cordillera. Arizona Geological Society Digest, v. 14, pp. 113–135.

Dickinson, W.R., 1985, Interpreting provenance from detrital modes of sandstones, *in* Zuffa, G.G., ed., *Provenance of Arenites*: Dordrecht, Netherlands, Reidel Publishing, p. 333–361, https://doi.org/10.1007/978-94-017-2809-6_15.

Dickinson, W.R., 1995, Forearc basins, in Busby, C.J., and Ingersoll, R.V., eds., Tectonics of Sedimentary Basins: Cambridge, Massachusetts, Blackwell, p. 221–261.

Dickinson, W. R., Hopson, C. A., and Saleeby, J. B.,1996a, Alternate Origins of the Coast Range Ophiolite (California): Introduction and Implications: GSA Today, v. 7, no 2.

Dickinson, W. R., Schweickert, R. A., and Ingersoll, R. V., 1996b, Coast Range Ophiolite as back-arc-inter-arc basin lithopshere. GSA Today, v. 6(2), pp. 2–4.

Dickinson, W.R., 2008. Accretionary Mesozoic–Cenozoic expansion of the Cordilleran continental margin in California and adjacent Oregon. Geosphere 4, 329–353

Dickinson, W.R., Gehrels, G.E., 2009. Use of U-Pb ages of detrital zircons to infer maximum depositional ages of strata: a test against a Colorado Plateau Mesozoic database. Earth and Planetary Science Letter 288, 115e125.

Dickinson, W.R., Lawton, T.F., Pecha, M., Davis, S.J., Gehrels, G.E., and Young, R.A., 2012, Provenance of the Paleogene Colton Formation (Uinta Basin) and Cretaceous–Paleogene provenance evolution in the Utah foreland: Evidence from U-Pb ages of detrital zircons, paleocurrent trends, and sandstone petrofacies: *Geosphere* , v. 8, p. 854–880, https://doi.org/10.1130/GES00763.1.

Dibblee, T.W., 1982, Stanislaus, California, n.d., 1. 2008

Dumitru, T.A., Wakabayashi, J., Wright, J.E., and Wooden, J.L., 2010, Early Cretaceous transition from nonaccretionary behavior to strongly accretionary behavior within the Franciscan subduction complex: Tectonics, v. 29, TC5001, https:// doi.org/10.1029/2009TC002542.

Dumitru, T.A., Ernst, W.G., Hourigan, J.K., and McLaughlin, R.J., 2015, Detrital zircon U-Pb reconnaissance of the Franciscan subduction complex in northwestern California: International Geology Review, v. 57, p. 767–800, doi:10.1080/00206814.2015.1008060.

Dumitru, T.A., Elder, W.P., Hourigan, J.K., Chapman, A.D., Graham, S.A., Wakabayashi, J., 2016. Four Cordilleran paleorivers that connected Sevier thrust zones in Idaho to depocenters in California, Washington, Wyoming, and, indirectly, Alaska. Geology 44, 75–78

Dumitru, T. A, Hourigan, J.K., Elder, W. P., Ernst, W. P., Joesten, R., 2018. "New, much younger ages for the Yolla Bolly terrane and a revised timeline for accretion in the Franciscan subduction complex, California", Tectonics, Sedimentary Basins, and Provenance: A Celebration of the Career of William R. Dickinson, Raymond V. Ingersoll, Timothy F. Lawton, Stephan A. Graham

Engebretson, D.C., Cox, A., and Gordon, R.G., 1985, Relative Motions between Oceanic and Continental Plates in the Pacific Basin: *Geological Society of America Special Paper* 206, 59 p, doi:10.1130/SPE206-p1, doi:10.1130/SPE206-p1.

Ernst, W.G., 1970, Tectonic contact between the Franciscan mélange and the Great Valley Sequence, crustal expression of a Late Mesozoic Benioff Zone: *Journal of Geophysical Research*, v. 75, p. 886–901, doi:10.1029/JB075i005p00886.

Evarts, R. C., 1977, The geology and petrology of the Del Puerto ophiolite, Diablo Range, central California Coast Ranges, in Coleman, R. G., and Irwin, W. P., eds., North American ophiolites: Oregon Department of Geology and Mineral Industries Bulletin 95, p. 121–139.

Evarts, R. C., and Schiffman, P., 1982, Submarine hydrothermal metamorphism of the Del Puerto ophiolite, California: American Journal of Science, v. 283, p. 289–340.

Evarts, R.C., Coleman, R.G., and Schiffman, P., 1999, The Del Puerto ophiolite: Petrology and tectonic setting, *in* Wagner, D.L., and Graham, S.A., eds., *Geologic Field Trips in Northern California; Centennial Meeting of the Cordilleran Section of the Geological Society of America, Special Publication 119* : Sacramento, California, Department of Conservation, Division of Mines and Geology, p. 136–149.

Evarts, R. C., 1992, The Del Puerto Canyon Remnant of the Great Valley Ophiolite: Geochemical and Age Constraints on its Formation and Evolution. AAPG Bulletin. 76. 10.1306/F4C8F354-1712-11D7-8645000102C1865D.

Evarts, R.C., 1978, The Del Puerto ophiolite complex. California: A structural and petrologic investigation: Ph.D. dissertation. Stanford University, Stanford, CA, 409p.

Fralick, P.W., 2003, Geochemistry of clastic sedimentary rocks: ratio techniques, *in* Lentz, D.R., ed., *Geochemistry of Sediments and Sedimentary Rocks: Evolutionary Considerations to Mineral Deposit-Forming Environments: Geological Association of Canada, GeoText 4*, p. 85–103.

Fuller, C.W., Willett, S.D., and Brandon, M.T., 2006, Formation of forearc basins and their influence on subduction zone earthquakes: Geology, v. 34, no. 2, p. 65–68, doi: 10.1130/G21828.1.

Galbraith, R. and Laslett, G. Statistical models for mixed fission track ages. *Nuclear tracks and radiation measurements*, 21(4):459–470, 1993.

Galbraith, R. Graphical display of estimates having differing standard errors. *Technometrics*, 30(3): 271–281, 1988.

Gazzi, P., 1966, "Le Arenarie del Flysch Sopracretaceo dell'Appennino Modenese: Correlazioni con il Flysch di Monghidoro". Mineralogica e Petrografica Acta 12:69 97.

Gehrels, G.E., 2003. AgePick. https://sites.google.com/a/laserchron.org/laserchron/ home/ (last accessed: May, 2018).

Gehrels, G. E., 2012, Detrital Zircon U-Pb Geochronology: Current Methods and New Opportunities, Tectonics of Sedimentary Basins, pp. 45–62., doi:10.1002/9781444347166.ch2.

Gehrels, G.E., 2014. Detrital zircon U-Pb geochronology applied to tectonics. Annual Review of Earth and Planetary Sciences 42, 127e149.

Gehrels, G., and Pecha, M., 2014, Detrital zircon U-Pb geochronology and Hf isotope geochemistry of Paleozoic and Triassic passive margin strata of western North America: *Geosphere*, v. 10, p. 49–65, doi:10.1130/GES00889.1.

Gehrels, G.E., Valencia, V.A. and Ruiz, J., 2008. Enhanced precision, accuracy, efficiency, and spatial resolution of U-Pb ages by laser ablation–multicollector–inductively coupled plasma–mass spectrometry. Geochemistry, Geophysics, Geosystems, 9(3).

Greene, T. J., Surpless, K. D.; Facies architecture and provenance of a boulder-conglomerate submarine channel system, Panoche Formation, Great Valley Group: A forearc basin response to middle Cretaceous tectonism in the California convergent margin. *Geosphere* 2017;; 13 (3): 838–869. doi: https://doi.org/10.1130/GES01422.1

Gerstenberger, H., Haase, G., 1997, A highly effective emitter substance for mass spectrometric Pb isotope ratio determinations: Chemical Geology 136: 309-312.

Hall, C. A., Jr., 1958, Geology and paleontology of the Pleasnton area, Alameda and Contra Costa Counties, California: University of the California Publications in Geological Sciences, vol. 34, no. 1, 89 pp.

Harper, G. D., and Wright, J. E., 1984, Middle to Late Jurassic tectonic evolution of the Klamath Mountains, California-Oregon: Tectonics, v. 3, p. 759-772.

Hassani, R., Jongmans, D., and Chéry, J., 1997, Study of plate deformation and stress in subduction processes using two-dimensional numerical models: Journal of Geophysical Research, v. 102, no. B8, p. 17,95117,965, doi:10.1029/97JB01354.

Herriott, T.M., Crowley, J.L., Schmitz, M.D., Wartes, M.A., and Gillis, R.J., 2019, Exploring the law of detrital zircon: LA-ICP-MS and CA-TIMS geochronology of Jurassic forearc strata, Cook Inlet, Alaska, USA: Geology, v. 47, p. 1044–1048, https://doi.org/10.1130/G46312.1.

Hessler, A.M., and Sharman, G.R., 2018, Subduction zones and their hydrocarbon systems: Geosphere, v. 14, p. 2044–2067, https://doi.org/10 .1130/GES01656.1.

Hofmann, A. W., 1997, Mantle geochemistry: the message from oceanic volcanism. Nature 385, p. 219-229, doi: 10.1038/385219a0

Hopson, C. A., Mattinson, J. M., Luyendyk, B. P., and Pessagno, E. A., Jr., 1991, California Coast Range Ophiolite (CRO): Middle Jurassic/central Tethyan and latest Jurassic/southern Boreal episodes of ocean-ridge magmatism: Eos (American Geophysical Union Transactions), v. 72, p. 443.

Hopson, C.A., Mattinson, J.M., and Pessagno, E.A.. Jr., 1981, Coast Range ophiolite, western California, in Ernst, W.G., ed. The geotectonic development of California, Rubev Volume I: Englewood Cliffs, N.J., Prentice Hall, p. 418-510.

Hopson, C., Pessagno, E.A.P., Jr., Mattinson, J., Luyendyk, B., Beebe, W., Hull, D., Munoz, E., and Blome, C., 1996, Coast Range ophiolite as paleoequatorial mid-ocean lithosphere, in Dickinson, W.R., Hopson, C.A., and Saleeby, J.B., Alternate Origins of the Coast Range ophiolite (California): Introduction and Implications: GSA Today, v. 6, no. 2, p. 4–6.

Hopson, C. A., Mattinson, J. M., Pessagno E. A., Luyendyk, B. P., 2008 California Coast Range ophiolite: Composite Middle and Late Jurassic oceanic lithosphere *in* Wright, J. E., and Shervais, J. W., eds., Ophiolites, Arcs and Batholiths: A Tribute to Cliff Hopson: The Geological Society of America, Special Paper 438, p. 1-101, doi: 10.1130/2008.2438(01).

Horstwood, M.S., Košler, J., Gehrels, G., Jackson, S.E., McLean, N.M., Paton, C., Pearson, N.J., Sircombe, K., Sylvester, P., Vermeesch, P. and Bowring, J.F., 2016. Community-derived standards for LA-ICP-MS U-(Th-) Pb geochronology–Uncertainty propagation, age interpretation and data reporting. Geostandards and Geoanalytical Research, 40(3), pp.311-332.

Huey, A. S., 1948, Geology of the Tesla quadrangle, California: California Division of Mines Bulletin 140, 75 pp.

Hull, D. M., Pessagno, E. A., Jr., Hopson, C. A., Blome, C. D., and Muñoz, I. M., 1993, Chronostratigraphic assignment of volcanopelagic strata above the Coast Range Ophiolite, in Dunne, G., and McDougall, K., eds., Mesozoic paleogeography of the western United States—II: Pacific Section SEPM Book 71, p. 151–170.

Ibañez-Mejia, M., Pullen, A., Pepper, M., Urbani, F., Ghoshal, G., and Ibañez-Mejia, J.C., 2018, Use and abuse of detrital zircon U-Pb geochronology—A case from the Río Orinoco delta, Eastern Venezuela: Geology, v. 46, p. 1019–1022, https://doi.org/10.1130 /G45596.1.

Imlay, R.W., and Jones, D.L., 1970, Ammonites from the Buchia zones in northwestern California and southwestern Oregon: U.S. Geological Survey Professional Paper 647-B, 55 p., https://doi.org /10.3133/pp647B.

Imlay, R.W., Dole, H.M., Peck, D.L., and Wells, F.G., 1959, Relations of certain Upper Jurassic and Lower Cretaceous formations in Southwestern Oregon: American Association of Petroleum Geologists Bulletin, v. 43, p. 2770–2785

Ingersoll, R. V., 1978, Petrofacies and petrologic evolution of the Late Cretaceous fore-arc basin, northern and central California. Journal of Geology, v. 86, pp. 335–352.

Ingersoll, R.V., 1982, Initiation and evolution of the Great Valley forearc basin of northern and central California, USA, in Leggett, J.K., ed., Trench-Forearc Geology: Sedimentation and Tectonics on Modern and Ancient Active Plate Margins: Geological Society of London Special Publication 10, p. 459–467, doi:10.1144/GSL.SP.1982.010.01.31.

Ingersoll, R. V., 1983, Petrofacies and provenance of Late Mesozoic forearc basin, northern and central California. American Association of Petroleum Geologists Bulletin, v. 67, pp. 1125–1142.

Ingersoll, R. V., Schweickert, R. A., 1986, A Plate Tectonics Model for Late Jurassic Ophiolite Genesis, Nevadan Orogeny and Forearc Initiation, Northern California, Tectonics, vol. 5, no. 6, p. 901-912

Ingersoll, R. V., 1979, Evolution of the Late Cretaceous forearc basin, northern and central California. Geological Society of America Bulletin, v. 90(Part I), pp. 813–826.

Ingersoll, R. V., 2000, Models for origin and emplacement of Jurassic ophiolites of northern California, in Dilek, Y., Moores, E. M., Elthon, D., and Nicolas, A. eds., Ophiolites and oceanic crust: new insights from field studies and the Ocean Drilling Program, Geological Society of America (Special Paper 349), pp. 395–402.

Ingersoll, R. V., 2019, Subduction Related Sedimentary Basins of the US Cordillera. The sedimentary basins of the United States and Canada, p. 477-510

Jacobson, C. E., Grove, M., Pedrick, J. N., Barth, A. P., 2011, Late Cretaceous-early Cenozoic tectonic evolution of the southern California margin inferred fro provenance of trench and forearc sediments; geological Society of America Bulletin, vol. 123(3-4), p. 485-506, DOI: 10.1120/B30238.1

Jaffey, A.H., Flynn, K.F., Glendenin, L.E., Bentley, W.C., Essling, A.M., 1971, Precision measurements of half-lives and specific activities of 235U and 238U: Physical Review C, 4: 1889-1906.

Jennings, C.W., with modifications by Gutierrez, C., Bryant, W., Saucedo, G., and Wills, C., 2010, Geologic map of California: California Geological Survey, Geologic Data Map Number 2, scale 1:750,000.

Johnson, D.M., Hooper, P.R., and Conrey, R.M., 1999, XRF analysis of rocks and minerals for major and trace elements on a single low dilution Li-tetraborate fused bead: *Advances in X-Ray Analysis* , v. 41, p. 843–867.

Jones, D.L., Bailey, E.H., and Imlay, R.W., 1969, Structural and stratigraphic significance of the Buchia zones in the Colyear Springs–Paskenta area, California: U.S. Geological Survey Special Paper 647-A, 21 p.

Karig, D.E., 1974, Evolution of arc systems in the western Pacific: Annual Review of Earth and Planetary Sciences, v. 2, no. 1, p. 51–75, doi:10 .1146/annurev.ea.02 .050174.000411.

Karig, D.E., and Sharman, G.F., III, 1975, Subduction and accretion in trenches: Geological Society of America Bulletin, v. 86, no. 3, p. 377–389, doi:10 .113/ 00016 - 7606(1975)86<377:SAAIT>2.0.CO;2.

Knaack, C., Cornelius, S.B., and Hooper, P.R., 1994, Trace element analyses of rocks and minerals by ICP-MS: http://cahnrs.wsu.edu/soe/facilities/geolab/technotes/icp-ms_method/ (Accessed 2016).

Krogh, T.E., 1973, A low contamination method for hydrothermal decomposition of zircon and extraction of U and Pb for isotopic age determination: Geochimica et Cosmochimica Acta 37: 485-494.

Lanphere, M. A., 1971, Age of Mesozoic Oceanic Crust in the California Coast Ranges: Geological Society of America Bulletin, v. 82, p. 3209-3212.

Larroque, C., Calassou, S., Malavieille, J., and Chanier, F., 1995, Experimental modelling of forearc basin development during accretionary wedge growth: Basin Research, v. 7, no. 3, p. 255–268, doi:10 .1111/j .1365 -2117.1995.tb00109.x.

Maddock, M. E., 1964, Geology of the Mt. Boarman quadrangle, Santa Clara and Stanislaus counties, California; California Division of Mines and Geology, map sheet 3, map scale 1:62,500.

Mansfield, C.F., 1979, Upper Mesozoic subsea fan deposits in the southern Diablo Range, California: record of the Sierra Nevada magmatic arc. Geological Society of America Bulletin, v. 90(Part I), pp. 1025–1046.

Mattinson, J.M., 2005, Zircon U-Pb chemical abrasion ("CA-TIMS") method: combined annealing and multi-step partial dissolution analysis for improved precision and accuracy of zircon ages: Chemical Geology 220:47-66.

Mattinson, J.M., and Hopson, C.A., 2008, New high-precision CA-TIMS U-Pb zircon plateau ages for the Point Sal and San Simeon ophiolite remnants, California Coast Ranges, in Wright, J.E., and Shervais, J.W., eds., Ophiolites, Arcs, and Batholiths: A Tribute to Cliff Hopson: Geological Society of America Special Paper 438, doi: 10.1130/2008.2438(02)

McLennan, S.M., Taylor, S.R., McCulloch, M.T., and Maynard, J.B., 1990, Geochemical and Nd-Sr isotopic composition of deep-sea turbidites: Crustal evolution and plate tectonic associations: *Geochimica et Cosmochimica Acta* , v. 54, p. 2015–2050, doi:10.1016/0016-7037(90)90269-Q.

McLennan, S.M., Hemming, S., McDaniel, D.K., and Hanson, G.N., 1993, Geochemical approaches to sedimentation, provenance, and tectonics, *in* Johnson, M.J., and Basu, A., eds., *Processes Controlling the Composition of Clastic Sediments* : Geological Society of America Special Paper 284, p. 21–40, doi:10.1130/SPE284-p21, doi:10.1130/SPE284-p 21.

McNulty, B.A., 1995, Shear zone development during magmatic arc construction: the Bench Canyon shear zone, central Sierra Nevada, California: Geological Society of America Bulletin, v. 107, p. 1094–1107, doi:10.1130/0016-7606(1995)107<1094:SZDDMA>2.3.CO;2.

Moores, E. M., 1970, Ultramafics and orogeny, with models of the US Cordillera and Tethys: Nature, v. 228, p. 837–842.

Moores, E. M., and Day, H. W., 1984, Overthrust model for Sierra Nevada: Geology, v. 12, p. 416–419

Moores, E., 1970, Ultramafics and orogeny, with models of the U.S. Cordillera and the Tethys: Nature, v. 228, p. 837-842.

Mountney, N.P., and Westbrook, G.K., 1997, Quantitative analysis of Miocene to Recent forearc basin evolution along the Colombian convergent margin: Basin Research, v. 9, no. 3, p. 177–196, doi:10 .1046/j .1365 -2117.1997.00040.x.

Moxon, I.W., 1990, Stratigraphic and structural architecture of the San Joaquin–Sacramento Basin [Ph.D. thesis]: Stanford, California, Stanford University, 371 p.

Mulcahy, S.R., Starnes, J.K., Day, H.W., Coble, M.A., and Vervoort, J.D., 2018, Early onset of Franciscan subduction: Tectonics, v. 37, p. 1194–1209, doi: 10.1029/2017tc004753.

Noda, A., 2016, Forearc basins: Types, geometries, and relationships to subduction zone dynamics: Geological Society of America Bulletin, v. 128, p. 879–895, https://doi.org/10.1130/B31345.1.

Ojakangas, R. W., 1968, Cretaceous Sedimentation, Sacramento Valley, California: Geological Society of America Bulletin, v. 79, p. 973-1008.

Okamura, Y., and Shishiskura, M., 2020, New hypothesis to explain Quaternary forearc deformation and the variety of plate boundary earthquakes along the Suruga-Nankai Trough by oblique subduction of undulations on the Philippine Sea Plate. Earth, Planets and Space. 72. 10.1186/s40623-020-01183-5

Orme, D. A, and Graham, S. A., 2018, Four-dimensional model of Cretaceous depositional geometry and sediment flux in the northern Great Valley forearc, California. Tectonics, Sedimentary Basins, and Provenance: A Celebration of the Career of William R. Dickinson, Raymond V. Ingersoll, Timothy F. Lawton, Stephan A. Graham

Orme, D.A., and Surpless, K.D., 2019, The birth of a forearc: The Basal Great Valley Group, California, USA: Geology, v. 47, p. 757–761, doi: 10.1130/g46283.1.

Page, B.M., and Engebretson, D.C., 1984, Correlation between the geologic record and computed plate motions for central California: *Tectonics*, v. 3, p. 133–155, doi:10.1029/TC003i002p00133.

Paterson, S.R., and Ducea, M.N., 2015, Arc magmatic tempos: *Gathering the evidence: Elements*, v. 11, p. 91–98, doi:10.2113/gselements.11.2.91.

Rai, P. and Matthew, G., 2021. Presence of detrital olivine and serpentine minerals in the Dihing unit of upper Assam: Implication towards the source. *J Earth Syst Sci* 130, 86 (2021). https://doi.org/10.1007/s12040-021-01581-7

Raymond, L. A., 1970, Cretaceous sedimentation and regional thrusting, northeastern Diablo Range, California; Geological Society of America Bulletin, v. 81, p. 2123-2128

Raymond, L. A., 1973, Tesla-Ortigalita Fault, Coast Range Thrust Fault, and Franciscan Metamorphism, Northeastern Diablo Range, California: Geological Society of American Bulletin, v. 84, p. 3547-3562

Robertson, A. H. F., 1989, Palaeoceanography and tectonic setting of the Jurassic Coast Range ophiolite, central California: Evidence from the extrusive rocks and the volcaniclastic sediment cover: Marine and Petroleum Geology, v. 6, p. 194–220.

Romero, M.C., Orme, D.A., Surpless, K.D., Ronemus, C.B., Morrow, Z., 2024, Age and provenance relationships between the basal Great Valley Group and its underlying basement: Implications for the development of the Great Valley forearc basin, California, *Journal of Sedimentary Research, in press.*

Ryan, K.M., and Williams, D.M., 2007, Testing the reliability of discrimination diagrams for determining the tectonic depositional environment of ancient sedimentary basins: Chemical Geology, v. 242, p. 103–125. doi:10.1016/j.chemgeo.2007.03.013

Saleeby, J. B., 1982, Polygenetic ophiolite belt of the California Sierra Nevada: Geochronological and tectonostratigraphic development: Journal of Geophysical Research, v. 87, p. 1803–1824.

Saleeby, J. B., 1992, Petrotectonic and paleogeographic settings of U.S. Cordilleran ophiolites, in Burchfiel, B. C., et al., The Cordilleran orogen: Conterminous U.S.: Boulder, Colorado, Geological Society of America, Geology of North America, v. G-3, p. 653–682.

Saleeby, J. B., Busby-Spera, C., Oldow, J., Dunne, G., Wright, J. E., Cowan, D., Walker, N., Allmendinger, R., 1992, Early Mesozoic tectonic evolution of the western U.S. Cordillera, in Burchfiel, B. C., et al., eds., The Cordilleran orogen: Conterminous U.S.: Boulder, Colorado, Geological Society of America, Geology of North America, v. G-3, p. 107–168.

Saleeby, J. B., and Harper, G. D., 1993, Tectonic relations between the Galice Formation and the schists of Condrey Mountain, Klamath Mountains, northern California, in Dunne, G., and McDougall, K., eds., Mesozoic paleogeography of the western United States—II: Pacific Section SEPM, Book 71, p. 61–80.

Saleeby, J.B., 1996, Coast Range ophiolite as parautochthonous forearc lithosphere: GSA Today, v. 6, no. 2, p. 6–8.

Schlüter, H. U., C. Gaedicke, H. A. Roeser, B. Schreckenberger, H. Meyer, C. Reichert, Y. Djajadihardja, and A. Prexl, Tectonic features of the southern Sumatra-western Java forearc of Indonesia, *Tectonics*, 21(5), 1047, doi:10.1029/2001TC901048, 2002.

Schmitz, M.D., Schoene, B., 2007, Derivation of isotope ratios, errors and error correlations for U-Pb geochronology using 205Pb-235U-(233U)-spiked isotope dilution thermal ionization mass spectrometric data: Geochemistry, Geophysics, Geosystems (G3) 8, Q08006, doi:10.1029/2006GC001492.

Scholl, D.W., von Huene, R., Vallier, T.L., and Howell, D.G., 1980, Sedimentary masses and concepts about tectonic processes at underthrust ocean margins: Geology, v. 8, no. 12, p. 564–568, doi:10.1130/0091-7613(1980)8 <564:SMACAT>2.0.CO;2.

Schweickert, R. A., and Cowan, D. S., 1975, Early Mesozoic tectonic evolution of the western Sierra Nevada, California: Geological Society of America Bulletin, v. 86, p. 1329–1336.

Schweickert, R.A., Bogen, N.I., Girty, G.H., Hanson, R.F., Merguerian, C., 1984. Timing and structural expression of the Nevadan orogeny, Sierra Nevada, California. Geol. Soc. Am. Bull. 95, 967–979.

Schweickert, R.A., 2015, Jurassic evolution of the Western Sierra Nevada metamorphic province, *in* Anderson, T.H., Didenko, A.N., Johnson, C.L., Khanchuk, A.I., and MacDonald, J.H., eds., *Late Jurassic Margin of Laurasia—A Record of Faulting Accommodating Plate Rotation*: Geological Society of America Special Paper 513, p. 299–358, doi:10.1130/2015.2513(08).

Seely, D.R., Vail, P.R., and Walton, G.G., 1974, Trench slope model, in Burk, C.A., and Drake, C.L., eds., The Geology of Continental Margins: New York, Springer-Verlag, p. 249–260, doi:10.1007/978-3-662-01141-6_18.

Sharman, G. R., Graham, S. A., Grove, M., Kimbrough, D. L., Wright, J. E., 2015, Detrital zircon provenance of the Late Creataceous-Eocene California forearc: Influence and

Laramide low-angle subduction on sediment dispersal and paleogeography, Geological Society of America, vol. 127, issue 1-2, p. 38-60

Shervais, J. W., and Kimbrough, D. L., 1985, Geochemical evidence for the tectonic setting of the Coast Range ophiolite: A composite island-arc–oceanic crust terrane in western California: Geology, v. 13, p. 35–38.

Shervais, J. W., 1990, Island arc and ocean crust ophiolites: Contrasts in the petrology, geochemistry and tectonic style of ophiolite assemblages in the California Coast Ranges, in Malpas, J., et al., eds., Ophiolites, oceanic crustal analogues: Nicosia, Cyprus Geological Survey Department, p. 507–520.

Shervais, J. W., Murchey, B. L., Kimbrough, D. L., Renne, P., Hanan, B. B., 2005, radioisotopic and biostratigraphic age relations in the Coast Range Ophiolite, northern Califronia: Implications for the tectonic evolution of the Western cordillera: GSA Bulletin, v. 117, n. 5/6, p. 633-653, doi:10.1130/B25443.1

Snow, C.A., Wakabayashi, J., Ernst, W.G., and Wooden, J.L., 2010, Detrital zircon evidence for progressive underthrusting in Franciscan metagraywackes, west-central California: *Geological Society of America Bulletin* , v. 122, p. 282–291, doi:10.1130/B26399.1.

Spencer, C.J., Kirkland, C.L., Taylor, R.J.M., 2016. Strategies towards statistically robust interpretations of in situ U-Pb zircon geochronology. Geoscience Frontiers 7, 581e589.

Stern, R.J., 2002, Subduction zones: Reviews of Geophysics, v. 40, no. 4, p. 1012, doi:10 .1029/2001RG000108.

Stern, C. 2004, Active Andean volcanism: its geologic and tectonic setting. Revista Geológica de Chile 31 (2): 161-206.

Sundell, K.E., Saylor, J.E., 2021. Two-dimensional quantitative comparison of density distributions in detrital geochronology and geochemistry. Geochem. Geophys. Geosyst. 22 (4), e2020GC009559.

Sundell, K.E., Gehrels, G.E. and Pecha, M.E., 2020, Rapid U-Pb Geochronology by Laser Ablation Multi- collector ICP-MS. Geostandards and Geoanalytical Research.

Surpless, K.D., Graham, S.A., Covault, J.A., and Wooden, J.L., 2006, Does the Great Valley Group contain Jurassic strata?: Reevaluation of the age and early evolution of a classic forearc basin: Geology, v. 34, p. 21–24, https://doi.org/10.1130/G21940.1.

Surpless, K.D., 2014, Geochemistry of the Great Valley Group: *An integrated provenance record: International Geology Review*, v. 57, p. 747–766, doi:10.1080/00206814.2014.923347.

Surpless, K.D., Clemmens-Knott, D., Barth, A. P., Gevedon, M., 2019, A survey of Sierra Nevada magmatism using Great Valley detrital zircon trace-elemet geochemistry: View from the forearc; Lithosphere, vol. 11, issue 5, p. 603-619.

Tagami, T. & Dumitru, T. A. 1996. Provenance and thermal history of the Franciscan accretionary complex: constraints from zircon fission track thermochronology. Journal of Geophysical Research, 101, 11353-11364

Taylor, S.R., and McLennan, S.M., 1985, The continental crust: Its composition and evolution: Oxford, U.K., Blackwell, 312 p.

Tharp, T.M., 1985, Numerical models of subduction and forearc deformation: Geophysical Journal of the Royal Astronomical Society, v. 80, no. 2, p. 419–437, doi:10 .1111/j.1365-246X.1985.tb05102.x.

Tikoff, B., and Greene, D., 1997, Stretching lineations in transpressional shear zones: An example from the Sierra Nevada Batholith, California: Journal of Structural Geology, v. 19, p. 29–39, doi: 10.1016/S0191-8141(96)00056-9.

Tobisch, O.T., Saleeby, J.B., Renne, P.R., McNulty, B., and Tong, W., 1995, Variations in deformation fields during development of a large volume magmatic arc, central Sierra Nevada, California: Geological Society of America Bulletin, v. 107, p. 148–166, doi:10.1130/0016-7606(1995)107 <0148:VIDFDD>2.3.CO;2. Vermeesch, P., 2012, On the visualization of detrital age distributions: Chemical Geology, v. 312, p. 190–194, doi:10.1016/j.chemgeo.2012.04.021

Tomek, F., Žák, J., Verner, K., Ježek, J., & Paterson, S. R. (2024). A complex interplay between pluton emplacement, tectonic deformation, and plate kinematics in the Cretaceous Sierra Nevada magmatic arc, California. *Tectonics*, 43, e2023TC007822. https://doi.org/10.1029/2023TC007822

Trop, J. M., Ridgeway, K. D., Manuszak, J. D., Layer, P., 2002, Mesozoic sedimentary-basin development on the allocthonous Wrangellia composite terrane, Wrangell Mountains basin, Alaska: A long-term record of terrane migration and arc construction. GSA Bulletin, 114 (6): 693–717. doi: https://doi.org/10.1130/0016-7606(2002)114<0693:MSBDOT>2.0.CO;2

Utsunomiya, M., Tamura, I., Nozaki, A. *et al.* Basin-wide erosion and segmentation of the Plio-Pleistocene forearc basin in central Japan revealed by tephro- and biostratigraphy. *Prog Earth Planet Sci* 10, 25 (2023). https://doi.org/10.1186/s40645-023-00558-y

Vermeesch, P., 2018, IsoplotR: a free and open toolbox for geochronology. Geoscience Frontiers, v.9, p 1479-1493, doi:10.1016/j.gsf.2018.04.001.

Vermeesch, P., 2021, Maximum depositional age estimation revisited: Geoscience Frontiers, v. 12, p. 843–850, https://doi.org/10.1016/j.gsf.2020.08.008.

Vervoort, J. D., 2014, Lu-Hf Dating: The Lu-Hf Isotope System: Encyclopedia of Scientific Dating Methods, pp. 1–20., doi:10.1007/978-94-007-6326-5_46-1.

Vickery, F. P., 1924, Structural dynamics of the Livermore region: Jour. Geology, v. 33, p. 608-628.

von Huene, R., and Scholl, D.W., 1991, Observations at convergent margins concerning sediment subduction, subduction erosion, and the growth of continental crust: Reviews of Geophysics, v. 29, p. 279–316, doi:10 .1029 /91RG00969.

Wakabayashi, J., Ghatak, A., and Basu, A.R., 2010, Tectonic setting of supra subduction zone ophiolite generation and subduction initiation as revealed through geochemistry and regional field relationships: Geological Society of America Bulletin, v. 122, p. 1548-1568 https//doi.org/10.1130/B30017.1

Wakabayashi, J., 2015, Anatomy of a subduction complex: Architecture of the Franciscan Complex, California, at multiple length and time scales: International Geology Review, v. 57, p. 669–746, https://doi.org/10.1080/00206814.2014.998728.

Williams, I. S,. 1997, U-Th-Pb Geochronology by Ion Microprobe: Applications of Microanalytical Techniques to Understanding Mineralizing Processes, pp. 1–35., doi:10.5382/rev.07.01.

Wills, C. J., Gutierrez, C., Perez, F. G., & Branum, D., 2015. A Next Generation VS30 Map for California Based on Geology and Topography. *Bulletin of the Seismological Society of America*, 105(6), 3083-3091. doi: 10.1785/0120150105. SCEC Contribution 8857

Worrall, D. M., 1981, Imbricate low-angle faulting in uppermost Franciscan rocks, South Yolla Bolly area, northern California. Geological Society of America Bulletin, 92, 703-729

Wyld, S. J., and Wright, J. E., 1988, The Devils Elbow ophiolite remnant and overlying Galice Formation: New constraints on the Middle to Late Jurassic evolution of the Klamath Mountains, California: Geological Society of America Bulletin, v. 100, p. 29–44.

Yang, X., and Gao, H., 2020. Segmentation of the Aleutian-Alaska subduction zone revealed by full-wave ambient noise tomography: Implications for the along-strike variation of volcanism. *Journal of Geophysical Research: Solid Earth*, 125, e2020JB019677. https://doi.org/10.1029/2020JB019677

APPENDICES

APPENDIX A

ALL SAMPLE INFORMATION

(THIS DATA CAN BE FOUND IN SUPPLEMENTAL MATERIAL TAB 1)

APPENDIX B

LAICPMS DETRITAL ZIRCON U-PB

(THIS DATA CAN BE FOUND IN SUPPLEMENTAL MATERIAL TAB 2)

APPENDIX C

MAXIMUM DEPOSITIONAL AGES

(THIS DATA CAN BE FOUND IN SUPPLEMENTAL MATERIAL TAB 3)

APPENDIX D

SANDSTONE MODAL ANALYSIS

(THIS DATA CAN BE FOUND IN SUPPLEMENTAL MATERIAL TAB 4)

APPENDIX E

ZIRCON EPISLON HAFNIUM

(THIS DATA CAN BE FOUND IN SUPPLEMENTAL MATERIAL TAB 5)

APPENDIX F

U-PB VERSUS TH/U ALL ZIRCON GRAINS

(THIS DATA CAN BE FOUND IN SUPPLEMENTAL MATERIAL TAB 6)

APPENDIX G

WHOLE ROCK GEOCHEMISTRY

(THIS DATA CAN BE FOUND IN SUPPLEMENTAL MATERIAL TAB 7)